Controllability and Stabilization for Herding a Robotic Swarm Using a Leader: A Mean-Field Approach

Karthik Elamvazhuthi, Zahi Kakish, Aniket Shirsat, and Spring Berman, *Member, IEEE*

***Abstract*—In this article, we introduce a model and a control approach for herding a swarm of "follower" agents to a target distribution among a set of states using a single "leader" agent. The follower agents evolve on a finite state space that is represented by a graph and transition between states according to a continuous-time Markov chain (CTMC), whose transition rates are determined by the location of the leader agent. The control problem is to define a sequence of states for the leader agent that steers the probability density of the forward equation of the Markov chain. For the case, when the followers are possibly interacting, we prove local approximate controllability of the system about equilibrium probability distributions. For the case, when the followers are noninteracting, we design two switching control laws for the leader that drive the swarm of follower agents asymptotically to a target probability distribution that is positive for all states. The first strategy is open-loop in nature, and the switching times of the leader are independent of the follower distribution. The second strategy is of feedback type, and the switching times of the leader are functions of the follower density in the leader's current state. We validate our control approach through numerical simulations with varied numbers of follower agents that evolve on graphs of different sizes, through a 3-D multirobot simulation in which a quadrotor is used to control the spatial distribution of eight ground robots over four regions, and through a physical experiment in which a swarm of ten robots is herded by a virtual leader over four regions.**

***Index Terms*—Feedback control, herding, Markov chains, multirobot systems, stabilization, swarms, switching systems.**

I. Introduction

We present a control strategy for herding a swarm of agents to a target distribution among a set of states using a single leader agent. For example, a leader with sophisticated sensing, localization, and planning capabilities may be required to herd a group of follower agents, which lack these capabilities, through an environment with obstacles. This control approach has a wide range of applications in swarm robotics, including exploration [34], environmental monitoring [14], debris clearance during disaster response [30], and targeted drug delivery at the micronanoscale [12], [23]. The ideas that we present in this article could also find applications for addressing problems other than those arising in swarm robotics, such as livestock herding [38] and crowd control [21].

There has been a considerable amount of work on control strategies in which a small number of leader robots guide a swarm of follower robots. Many of these strategies have been designed for containment control problems [20], in which the objective is to design interaction rules between the leaders and follower agents so that the followers are eventually contained in the convex hull spanned by the leaders. Most containment control approaches are based on multiagent consensus protocols [28], in which the leaders have an attractive effect on the followers. On the other hand, there have been few works on multirobot herding strategies in which the leaders have a repulsive effect on the followers. In [32] and [33], the authors consider a scenario with multiple noncooperative herders and establish stability guarantees for their control law by reducing the system to a unicycle model. This approach has been extended in [11] to construct controllers that are finite-time stabilizing. Control strategies for herding swarms with a single leader agent have also been proposed. For example, Haque *et al.* [19] presented control laws that are inspired by hunting strategies used by groups of bottlenose dolphins. It was shown in [7] that a single leader can herd a diffusive swarm, modeled with differential inclusions, by following open-loop sinusoidal trajectories. Similarly, we have shown in [16] that a single leader can herd a swarm of double-integrator agents, modeled with ordinary differential equations (ODEs), along a given smooth path by moving along appropriately designed oscillatory trajectories. Herding strategies that employ a single leader have also been considered in a feedback control framework using algorithm-constructed feedback laws [29] and switching adaptive laws [25].

In this article, we present a herding strategy that uses a single leader agent and is scalable with the number of follower agents. In our strategy, the follower agents switch between states according to a CTMC, which allows us to represent the dynamics of the probability distribution of followers over the states as a

Manuscript received April 25, 2020; accepted September 15, 2020. Date of publication October 28, 2020; date of current version April 2, 2021. This work was supported by ONR Young Investigator Award N00014-16-1-2605, and in part by the Arizona State University Global Security Initiative. This article was recommended for publication by Associate Editor M. Schwager and Editor P. Robuffo upon evaluation of the reviewers' comments. *(Corresponding author: Karthik Elamvazhuthi.)*

Karthik Elamvazhuthi is with the Department of Mathematics, University of California, Los Angeles, CA 90095 USA (e-mail: karthikevaz@math.ucla.edu).

Zahi Kakish, Aniket Shirsat, and Spring Berman are with the School for Engineering of Matter, Transport, and Energy, Arizona State University, Tempe, AZ 85287 USA (e-mail: zahi.kakish@asu.edu; ashirsat@asu.edu; spring.berman@asu.edu).

This article has supplementary downloadable material available at http://ieeexplore.ieee.org, provided by the authors.

Color versions of one or more of the figures in this article are available online at http://ieeexplore.ieee.org.

Digital Object Identifier 10.1109/TRO.2020.3031237

mean-field model in the form of a set of ODEs. The control parameters of this model are the followers' transition rates out of their current state. These transition rates are positive whenever the leader is present in the followers' current state. This specification causes the leader to have a "repulsive" effect on the followers. The scalability of this control approach arises from the fact that the mean-field model represents the swarm of followers as a continuum, and is therefore independent of the number of followers. In addition, the model control parameters define control laws that are used by all followers and are therefore independent of the followers' identities. For the case, where the followers are interacting, for example, through collision avoidance or aggregation type behaviors, we prove local approximate controllability of this system with the leader's position as the control parameter. Then, for the case of noninteracting followers, i.e., the transition rates are only a function of the leader's state, we construct a feedback control law for the leader that drives the followers to a given target probability distribution that is positive for all states. We validate our control strategy using numerical simulations, a 3-D multirobot simulation in which a quadrotor herds 8 small ground robots, and an experiment in which a virtual projected leader herds 10 physical robots.

Mean-field models of the type, we consider have previously been used in the design of stochastic control strategies for task allocation and spatial coverage by robotic swarms, e.g., in [1], [2], [4], [8], [26], and [27]. See [15] for a recent survey by the authors of works that use mean-field models for control problems in swarm robotics. These techniques contrast with classical approaches to multiagent control [28], in which the control laws depend on the individual agents' identities. This article extends this prior work by proposing a novel application of mean-field modeling in a leader–follower control problem for robotic swarms. Moreover, while prior work [1], [2], [4], [8], [26], [27] addresses control problems in which the transition rates or transition probabilities can be independently specified, we consider a more constrained control problem in which all transitions leaving a state have the same transition rate, since follower agents that are in the leader's current state can switch to any neighboring state with equal probability. We, therefore, demonstrate that the swarm's distribution can be controlled using a smaller number of control parameters than in previous works. In addition, our inclusion of a leader agent allows us to avoid the requirement that the agents of the swarm have global localization.

Comparison with prior work on herding: Most previous works on herding [7], [16], [19], [20], [29], [33] are limited to control strategies that ensure that the followers are confined to a small region in space. On the other hand, in this article, we present control strategies that herd the swarm to a larger class of follower distributions. While the control strategy presented in [24] and [25] can herd the set of followers to arbitrary configurations, it requires the leader to broadcast commands to each robot in the swarm indicating whether the follower is supposed to be in a *chased* or *unchased* mode. For such a leader–follower communication protocol to be implementable, the leader must be able to distinguish between different follower robots. The leader might not have such a capability in practice when the swarm is large. In contrast, in our approach, the leader does not directly communicate with the swarm of followers, and the followers do not have identities. Moreover, the control law in [24] and [25] requires the leader to switch its position between individual follower robots. Such a switching control law would scale poorly with the number of followers. On the other hand, the control laws that we present require the leader to switch its position between vertices of the graph that represent spatial states. The number of switchings in our control laws is a function of the number of possible states of a single follower, rather than the number of followers as in [24] and [25]. These properties ensure that our control laws scale well with the number of follower agents, as we verify through numerical simulations.

To summarize, the following are the *main contributions of this article*.

1) Introduction of a mean-field model for herding a swarm of unidentified (unlabeled) follower robots using a single leader that has a repulsive effect on the robots (see Section III).
2) Proof of local approximate controllability of the mean-field model about equilibrium (probability) distributions of the swarm, with the leader's position as the control input (see Theorem IV.4).
3) Global (practical) asymptotic stability result for a novel open-loop switching controller that stabilizes the swarm to a neighborhood of a given equilibrium distribution (see Theorem V.2).
4) Global asymptotic stability result for a novel closed-loop switching controller that stabilizes the swarm to a given equilibrium distribution (see Theorem V.8).

This article is organized as follows. In Section II, we establish notation and provide some definitions that are used throughout this article. In Section III, we formulate the main problems that are addressed in this article. In Section IV, we present a detailed analysis of the controllability properties of the systems defined in Section III. In Section V, we consider the problem of stabilizing target equilibrium densities. In Sections VI–VIII, we validate the control strategies presented in Section V through numerical simulations, 3-D simulations, and physical experiments. Section IX concludes this article.

II. Notation

We first define some notation that will be used to formally state the problems addressed in this article. We will use the following definitions from graph theory. We denote by $\mathcal{G} = (\mathcal{V}, \mathcal{E})$ a directed graph with a set of M vertices, $\mathcal{V} = \{1, \ldots, M\}$, and a set of $N_{\mathcal{E}}$ edges, $\mathcal{E} \subset \mathcal{V} \times \mathcal{V}$, where $e = (i, j) \in \mathcal{E}$ if there is an edge from vertex $i \in \mathcal{V}$ to vertex $j \in \mathcal{V}$. We define a *source map* $S : \mathcal{E} \to \mathcal{V}$ and a *target map* $T : \mathcal{E} \to \mathcal{V}$ for which $S(e) = i$ and $T(e) = j$, whenever $e = (i, j) \in \mathcal{E}$. There is a *directed path* of length s from a vertex $i \in \mathcal{V}$ to a vertex $j \in \mathcal{V}$ if there exists a sequence of edges $\{e_i\}_{i=1}^{s}$ in $\mathcal{E}$ such that $S(e_1) = i, T(e_s) = j$, and $S(e_k) = T(e_{k-1})$ for all $2 \leq k \leq s$. A directed graph $\mathcal{G} = (\mathcal{V}, \mathcal{E})$ is called *strongly connected* if for every pair of distinct vertices v_0, $v_T \in \mathcal{V}$, there exists a *directed path* of edges in $\mathcal{E}$ connecting v_0 to v_T. We will assume that $(i, i) \notin \mathcal{E}$ for all $i \in \mathcal{V}$. For a given vertex $v \in \mathcal{V}$, we will denote the neighborhood of v by $\mathcal{N}(v) = \{w \in \mathcal{V};\ \exists e \in \mathcal{E}\ \text{s.t.}\ e = (v, w)\}$. The graph $\mathcal{G}$ is

said to be *bidirected* if $(v,w)\in\mathcal{E}$ implies that $(w,v)\in\mathcal{E}$ for all $v,w\in\mathcal{V}$. The cardinality of the set $\mathcal{N}(v)$ will be denoted by $|\mathcal{N}(v)|$. The vector $\mathbf{1}\in\mathbb{R}^M$ will be used to refer to the M-dimensional vector with all elements equal to 1. Given a vector $\mathbf{x}\in\mathbb{R}^M$, x_i will refer to the ith coordinate value of $\mathbf{x}$. The two-norm of the vector $\mathbf{x}\in\mathbb{R}^M$ will be denoted by $\|\mathbf{x}\|=\sqrt{\sum_i x_i^2}$. For a matrix $\mathbf{A}\in\mathbb{R}^{M\times N}$, A^{ij} will refer to the element in the ith row and jth column of $\mathbf{A}$.

A function $\mathbf{f}:\mathbb{R}\to\mathbb{R}^M$ is said to be absolutely continuous if $\forall\epsilon>0$, there exists $\delta>0$ such that for any finite set of disjoint intervals $(a_1,b_1),\ldots,(a_N,b_N)$, $\sum_{j=1}^N(b_j-a_j)<\delta\Rightarrow\sum_{j=1}^N\|\mathbf{f}(b_j)-\mathbf{f}(a_j)\|<\epsilon$. More generally, $\mathbf{f}$ is said to be absolutely continuous on $[a,b]$ if this condition is satisfied whenever the intervals (a_j,b_j), $j=1,\ldots,N$, all lie in $[a,b]$.

III. Problem Formulation

We consider a swarm of N follower agents and a single leader agent. All agents' states evolve in continuous time over the set $\mathcal{V}=\{1,\ldots,M\}$, which we represent as the vertices of a graph $\mathcal{G}$. The vertices in $\mathcal{V}$ represent a set of spatial locations obtained by partitioning the agents' environment. The edge set $\mathcal{E}$ defines the pairs of vertices between which the agents can transition. We will assume that the graph $\mathcal{G}=(\mathcal{V},\mathcal{E})$ is strongly connected. The leader agent performs a sequence of deterministic transitions from one vertex to another. The leader's location at time t is denoted by $\ell(t)\in\mathcal{V}$. The location of each follower agent $i\in\{1,\ldots,N\}$ is defined by a Markov chain $X_i(t)$ that evolves on the state space $\mathcal{V}$ according to the conditional probabilities

$$\begin{aligned}&\mathbb{P}(X_i(t+h)=T(e)|X_i(t)=S(e))=u_e(t)h+o(h)\\&\mathbb{P}(X_i(t+h)=v|X_i(t)=v)=1-\sum_{e\in\mathcal{E};S(e)=v}u_e(t)h+o(h)\end{aligned}\tag{1}$$

for each $e\in\mathcal{E}$. Here, h is an infinitesimally small time interval, $o(h)$ is the little-oh symbol, and $\mathbb{P}$ is the underlying probability measure induced on the space of events Ω by the stochastic processes $\{X_i(t)\}_{i=1}^N$. The first equation in (1) defines the probability of an agent jumping to a state $T(e)$ at time $t+h$, given that it is in the state $S(e)$ at time t. Similarly, the second equation in (1) defines the probability that an agent in state v at time t stays in this state at time $t+h$. Since h is infinitesimally small, the probability of the agent staying in the set $\mathcal{V}$ is equal to 1, which is consistent with our assumption that agents do not exit $\mathcal{V}$.

The fraction, or *empirical distribution*, of follower agents that are at location $v\in\mathcal{V}$ at time t is given by $\frac{1}{N}\sum_{i=1}^N\chi_v(X_i(t))$, where $\chi_v(w)=1$ if $w=v$ and 0 otherwise. Our goal is to design a control law that navigates the leader between vertices such that the follower agents are redistributed ("herded") from their initial empirical distribution $\frac{1}{N}\sum_{i=1}^N\chi_v(X_i(0))$ among the vertices to a desired empirical distribution $\frac{1}{N}\sum_{i=1}^N\chi_v(X_i(T))$ at some final time T, where T is a given finite number (controllability problem) or is infinite (stabilization problem). Since the identities of the follower agents are not important, we aim to construct a control policy for the leader that is a function of the current empirical distribution $\frac{1}{N}\sum_{i=1}^N\chi_v(X_i(t))$, rather than the individual agent states $X_i(t)$. However, $\frac{1}{N}\sum_{i=1}^N\chi_v(X_i(t))$ is not a state variable of the CTMC. In order to treat $\frac{1}{N}\sum_{i=1}^N\chi_v(X_i(t))$ as the state, we consider the *mean-field limit* of this quantity as $N\to\infty$. Let $\mathcal{P}(\mathcal{V})=\{\mathbf{y}\in\mathbb{R}^M_{\geq0};\sum_{v=1}^M y_v=1\}$ be the simplex of probability densities on $\mathcal{V}$. Under particular conditions that are discussed in the paragraph after Problem III.2, when $N\to\infty$, the empirical distribution $\frac{1}{N}\sum_{i=1}^N\chi_v(X_i(t))$ converges to the vth entry $x_v(t)$ of a deterministic quantity $\mathbf{x}(t)\in\mathcal{P}(\mathcal{V})$. Each entry $x_v(t)$ of the vector $\mathbf{x}(t)$ denotes the fraction of follower agents in state $v\in\mathcal{V}$ at time t. This vector evolves in time according to the following *Kolmogorov forward equation* or *mean-field model*, a system of ODEs, defined for $t\in[0,\infty)$

$$\dot{\mathbf{x}}(t)=\sum_{e\in\mathcal{E}}u_e(t)\mathbf{B}_e\mathbf{x}(t),\quad\mathbf{x}(0)=\mathbf{x}^0\in\mathcal{P}(\mathcal{V})\tag{2}$$

where $\mathbf{B}_e$ are control matrices whose entries are given by

$$B_e^{ij}=\begin{cases}-1 & \text{if } i=j=S(e)\\ 1 & \text{if } i=T(e),\ j=S(e)\\ 0 & \text{otherwise.}\end{cases}$$

The transition rates $u_e(t)$ are determined by the leader's location $\ell(t)$. In particular, for each $e\in\mathcal{E}$ and each $t\geq0$, we set

$$u_e(t)=\begin{cases}\eta+u_e^0(\mathbf{x}(t)) & \text{if } S(e)=\ell(t)\\ u_e^0(\mathbf{x}(t)) & \text{otherwise}\end{cases}$$

for a positive constant $\eta>0$ and a set of Lipschitz functions $u_e^0:\mathcal{P}(\mathcal{V})\to\mathbb{R}_{\geq0}$, which model interfollower interactions. The parameter η models the sensitivity of the follower agents to the leader's presence in their state. Higher values of η indicate that the follower agents transition out of their states at higher probability rates. For the purpose of analysis, without loss of generality, we will set $\eta=1$. The functions $u_e^0(\cdot)$ could, for example, be used to model an attractive effect between followers by setting $u_e^0(\mathbf{x})=x_{T(e)}$, where $x_{T(e)}$ denotes the fraction of agents in the state $T(e)$. Alternatively, $u_e^0(\cdot)$ could model *congestion effects* by setting $u_e^0(\mathbf{x})=0$ whenever $x_{T(e)}$ exceeds some threshold value. See Fig. 1 for an illustration of the agents' states and the interactions between the followers and the leader.

Then, for a given leader trajectory $\ell:\mathbb{R}_{\geq0}\to\mathcal{V}$, the system (2) can be rewritten as

$$\begin{aligned}&\dot{\mathbf{x}}(t)=\sum_{e\in\mathcal{E}}u_e^0(\mathbf{x}(t))\mathbf{B}_e\mathbf{x}(t)+\mathbf{D}_{\ell(t)}\mathbf{x}(t),\quad t\in[0,\infty)\\&\mathbf{x}(0)=\mathbf{x}^0\in\mathcal{P}(\mathcal{V})\end{aligned}\tag{3}$$

where, for each $v\in\mathcal{V}$, the matrix $\mathbf{D}_v\in\mathbb{R}^{N\times N}$ is given by

$$\mathbf{D}_v=\sum_{e\in\mathcal{E},S(e)=v}\mathbf{B}_e.\tag{4}$$

We make the following *assumptions about the agents' capabilities* for the case of noninteracting agents (i.e., $u_e^0=0$ for all $e\in\mathcal{E}$).

1) The leader can perfectly localize itself in $\mathcal{V}$; i.e., it knows its location $l(t)\in\mathcal{V}$ at each time t.

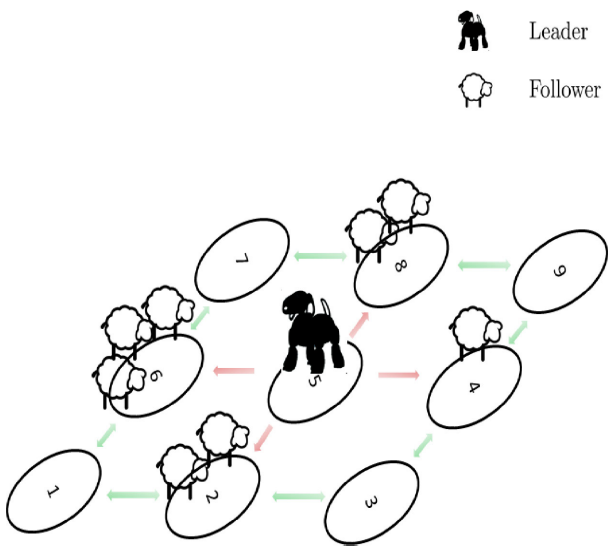

Fig. 1. Representation of the leader and follower agents' states for an example scenario with a bidirected grid graph $\mathcal{G}$. Green edges define the admissible transitions between states; red edges mean that the repulsive effect of the leader will cause the followers to exit the source state to the target states with positive transition rates.

2) The leader can measure the density of follower agents $x_{l(t)}(t)$ that are at its current location $l(t)$ at time t.
3) Each follower can sense whether the leader is present at the follower's current location.

We can now state the control problems that we address in this article. The first problem relates to the controllability of system (3).

Problem III.1: Given a target probability distribution $\mathbf{x}^{eq} \in \mathcal{P}(\mathcal{V})$ among the states in $\mathcal{V}$, and a time $T > 0$, construct a trajectory $\ell : [0, T] \to \mathcal{V}$ of the leader agent such that $\mathbf{x}(T) = \mathbf{x}^{eq}$.

After addressing the controllability problem, we will construct solutions for the following stabilization problem.

Problem III.2: Given a target probability distribution $\mathbf{x}^{\text{eq}} \in \mathcal{P}(\mathcal{V})$ among the states in $\mathcal{V}$, design the leader agent's trajectory $\ell : \mathbb{R}_{\geq 0} \to \mathcal{V}$ so that $\lim_{t\to\infty} \mathbf{x}(t) = \mathbf{x}^{\text{eq}}$.

By addressing Problems III.1 and III.2, we can synthesize a control input $\ell(t)$ for the mean-field model (3) that we can use to control the distribution of a large swarm of follower agents. We note that the mean-field model represents the swarm of followers as an infinite population, but in practice, the number of followers will be finite. Therefore, the applicability of solutions of Problems III.1 and III.2 to finite populations of follower agents depends on whether, for given transition rates $u_e(t)$, the empirical distribution $\frac{1}{N}[\sum_{i=1}^{N} \chi_1(X_i(t)) \dots \sum_{i=1}^{N} \chi_M(X_i(t))]^T$ of the N-agent Markov chain converges to the solution $\mathbf{x}(t)$ of the mean-field model (3) as $N \to \infty$; i.e., whether its mean-field limit is $\mathbf{x}(t)$. When the random variables $X_i(t)$ are independent, this convergence result follows trivially from the *law of large numbers*. However, if the transition rates $u_e(t)$ are functions of the density $\mathbf{x}(t)$, which is the case when there are interactions between followers, or if the leader's trajectory $\ell(t)$ is a function of the follower agent distribution, then the random variables $X_i(t)$ that represent the follower agents' states would not necessarily be independent. In this case, it would require significant work to determine whether the mean-field limit of the empirical distribution of followers is indeed the vector $\mathbf{x}(t)$; such an analysis is beyond the scope of this article.

Remark III.3: (Invariance of $\mathcal{P}(\mathcal{V})$) The total number of follower agents in the state space $\mathcal{V}$ should not change with respect to the transition rates $u_e(t)$. For the solution $\mathbf{x}(t)$ of the system (2), this implies that if $\mathbf{x}^0 \in \mathcal{P}(\mathcal{V})$, then we must have that $\mathbf{x}(t) \in \mathcal{P}(\mathcal{V})$ for all $t \in \mathbb{R}$. This property is automatically satisfied by solutions $\mathbf{x}(t)$ of the system (2) given the definitions of $\mathbf{B}_e$ and $u_e(t)$. In particular, since $\mathbf{1}^T\mathbf{B}_e = \mathbf{0}$, we have that $\mathbf{1}^T\dot{\mathbf{x}}(t) = \sum_{v=1}^{M} \dot{x}_v(t) = 0$ for all $t \geq 0$, and hence the mass of follower agents is always conserved. Moreover, both the transition rates $u_e(t)$ and all the off-diagonal entries of $\mathbf{B}_e$ are nonnegative. Hence, $\dot{x}_v(t) \geq 0$ for each $v \in \mathcal{V}$ such that $x_v(t) = 0$ whenever $\mathbf{x}(t)$ is nonnegative. Since the solutions $\mathbf{x}(t)$ are continuous, this implies that if $\mathbf{x}^0$ is nonnegative, then $\mathbf{x}(t)$ is nonnegative for all t.

IV. Controllability Analysis

In this section, we will address Problem III.1. It is a standard approach in control theory literature [10], [37] to study controllability properties of switched systems of the form (3) using controllability properties of a related *relaxed system*. The controllability results in [10] and [37] are restricted to bilinear systems. Since system (3) is not bilinear in general, we will perform our controllability analysis using the concept of *relaxed controls* [17], [40]. The approach of using relaxed controls to study controllability properties of herding models was first performed in [13], where the authors studied the reachability properties of the differential inclusion based herding model that was initially presented in [7]. In contrast to the models presented in [7] and [13], where the swarm of followers was represented as a subset of a Euclidean space, in our work, the swarm is represented as a probability distribution. Following this approach, we first prove the controllability of the following relaxed system:

$$\begin{aligned} \dot{\mathbf{y}}(t) &= \sum_{e\in\mathcal{E}} u_e^0(\mathbf{y}(t))\mathbf{B}_e\mathbf{y}(t) + \sum_{v\in\mathcal{V}} \alpha_v(t)\mathbf{D}_v\mathbf{y}(t) \\ &\quad t \in [0, \infty) \\ \mathbf{y}(0) &= \mathbf{x}^0 \in \mathcal{P}(\mathcal{V}) \end{aligned} \tag{5}$$

where $\alpha_v(t)$ is a nonnegative function for each $v \in \mathcal{V}$.

If system (5) is controllable with $\boldsymbol{\alpha}(t) = [\alpha_1(t) \dots \alpha_M(t)]^T$ as the control inputs, then it can be concluded that system (3) is controllable. In order to establish controllability of the relaxed system (5), we will show that the span of the set $\cup_{v\in\mathcal{V}}\{\mathbf{D}_v\mathbf{x}\}$ is equal to $M - 1$ for all $\mathbf{x} \in \mathcal{P}(\mathcal{V})$. To conclude this, we will use some spectral properties of $\mathbf{Q} := \sum_{v\in\mathcal{V}} \mathbf{D}_v = \sum_{e\in\mathcal{E}} \mathbf{B}_e$ that can be established using the *Perron–Frobenius theorem* [3] for positive matrices. These properties are stated in Lemma IV.1 below. Here and in the following sections, we define $\text{int}\,\mathcal{P}(\mathcal{V}) = \{\mathbf{x} \in \mathcal{P}(\mathcal{V}); x_v > 0\, \forall v \in \mathcal{V}\}$.

Lemma IV.1 (see [4]): The matrix $\mathbf{Q}$ has rank $M-1$ with 0 as its principal eigenvalue. Moreover, there exists $\boldsymbol{\beta} \in \operatorname{int} \mathcal{P}(\mathcal{V})$ such that $\mathbf{Q}\boldsymbol{\beta} = \mathbf{0}$.

Proof: See [4, Th. 1]. ■

We now establish local controllability of system (5) in the following lemma.

Lemma IV.2: Let $\mathbf{z} \in \operatorname{int} \mathcal{P}(\mathcal{V})$ be an equilibrium point of the system (5) with steady-state control input $\boldsymbol{\alpha}^{ss} = [\alpha_1^{ss} \dots \alpha_M^{ss}]^T \in \operatorname{int} \mathcal{P}(\mathcal{V})$. Let $T > 0$ be given and let $c = \min\{\alpha_i^{ss}; i \in \{1, \dots, M\}\}$. Then, there exists a neighborhood U of $\mathbf{z}$ in $\mathcal{P}(\mathcal{V})$ such that for each $\mathbf{x}^0 \in U$, there exists a set of measurable functions $\tilde{\alpha_v} : [0,T] \to [-c, c]$, such that $\sum_{v\in\mathcal{V}} \tilde{\alpha_v}(t) = 0$ for almost every $t \in [0,1]$ and the solution $\mathbf{x}(t)$ of the system (5) satisfies $\mathbf{x}(T) = \mathbf{z}$, with $\alpha_v(t) = \tilde{\alpha_v}(t) + \alpha_v^{ss}$ for all $v \in \mathcal{V}$ and almost every $t \in [0,T]$.

Proof: We will show that the set

$$A^{\mathbf{z}} = \left\{ \sum_{v\in\mathcal{V}} \gamma_v \mathbf{D}_v \mathbf{z};\ [\gamma_1 \dots \gamma_M]^T \in \mathbb{R}^M,\ \sum_{v\in\mathcal{V}} \gamma_v = 0 \right\}$$

is an $(M-1)$–dimensional subspace of $\mathbb{R}^M$. This would imply that (5) is *locally controllable* at $\mathbf{z}$ on $\mathcal{P}(\mathcal{V})$; i.e., there is a neighborhood U of $\mathbf{z}$ in $\mathcal{P}(\mathcal{V})$ in which system (5) is controllable to $\mathbf{x}^{\text{eq}}$.

According to Lemma IV.1, the matrix $\mathbf{Q}$ has rank $M-1$. Moreover, there exists $\boldsymbol{\beta} = [\beta_1 \dots \beta_M] \in \operatorname{int} \mathcal{P}(\mathcal{V})$ such that $\mathbf{Q}\boldsymbol{\beta} = \mathbf{0}$. Note that $\mathbf{D}_v \mathbf{z} = z_v (\mathbf{D}_v)^v$, where $(\mathbf{D}_v)^v$ denotes the vth column of $\mathbf{D}_v$. Therefore, we can conclude that the set

$$A_r^{\mathbf{z}} = \left\{ \sum_{v\in\mathcal{V}} \gamma_v \mathbf{D}_v \mathbf{z};\ [\gamma_1 \dots \gamma_M]^T \in \mathbb{R}^M \right\}$$

has dimension $M-1$. Let $\mathbf{y} = \sum_{v\in\mathcal{V}} \gamma_v \mathbf{D}_v \mathbf{z}$ be an element of $A_r^{\mathbf{z}}$ for some $[\gamma_1 \dots \gamma_M] \in \mathbb{R}^M$. Suppose that $\sum_{v\in\mathcal{V}} \gamma_v = c$. Then setting $\eta_v = \gamma_v - \frac{c\beta_v}{x_v \sum_{w\in\mathcal{V}} \beta_w}$ for each $v \in \mathcal{V}$, we note that $\mathbf{y} = \eta_v \mathbf{D}_v \mathbf{z}$ and $\sum_{w\in\mathcal{V}} \eta_w = 0$. This implies that $A^{\mathbf{z}} = A_r^{\mathbf{z}}$, and hence the set $A^{\mathbf{z}}$ is an $(M-1)$–dimensional subspace of $\mathbb{R}^M$. This implies that there are a sufficient number of *control directions* for system (5) on the $(M-1)$–dimensional submanifold $\mathcal{P}(\mathcal{V})$ in a neighborhood of $\mathbf{z}$. ■

In the next result, we establish that solutions of the relaxed system (5) can be approximated arbitrarily well using solutions of system (3). This will enable us to establish approximate controllability of system (3) in Theorem IV.4. In order to prove this result, we will need some new definitions and terminologies from measure theory [6]. Let $C(\mathcal{V})$ denote the space of functions on $\mathcal{V}$. We observe that, for the standard discrete topology on $\mathcal{V}$, all the functions in $C(\mathcal{V})$ are continuous. The space $L^1(0,T;C(\mathcal{V}))$ is defined by

$$L^1(0,T;C(\mathcal{V})) = \{f : (0,T) \to C(\mathcal{V}) \text{ is a measurable function; } \int_0^T \|f(t)\|_\infty dt < \infty\} \tag{6}$$

where $\|f(t)\|_\infty$ denotes the maximum of the function $f(t) \in C(\mathcal{V})$ attained over $\mathcal{V}$. We will also need the space $R(0,T;\mathcal{V})$, which will denote the set of *relaxed controls*; i.e., the set of elements e for which $e(t)$ is a probability measure on C for almost every $t \in (0,T)$. Since the set $\mathcal{V}$ has finite cardinality, we can identify the set of probability measures on $\mathcal{V}$ with $\mathcal{P}(\mathcal{V})$. Thus, if μ is a relaxed control, there exists a time-dependent vector-valued function $\boldsymbol{\alpha}(t) = [\alpha_1(t) \dots \alpha_v(t)]^T$ such that $\mu(t, \mathcal{U}) = \sum_{v\in\mathcal{U}} \mu(t, \{v\}) = \sum_{v\in\mathcal{U}} \alpha_v(t)$ for almost every $t \in (0,T)$ and all $\mathcal{U} \subset \mathcal{V}$. Then, the solution of the system (5) coincides with the solution of the system

$$\begin{aligned} \dot{\mathbf{z}}(t) &= \sum_{e\in\mathcal{E}} u_e^0(\mathbf{z}(t)) \mathbf{B}_e \mathbf{z}(t) + \int_{\mathcal{V}} \mathbf{D}_v \mathbf{y}(t) \mu(t, dv) \\ &\qquad t \in [0, \infty) \\ \mathbf{x}(0) &= \mathbf{x}^0 \in \mathcal{P}(\mathcal{V}). \end{aligned} \tag{7}$$

This implies that we can identify $R(0,T;\mathcal{V})$ with the set of elements in $L^\infty(0,1;\mathcal{P}(\mathcal{V}))$, the set of measurable functions defined over (0,1) that take values in $\mathcal{P}(\mathcal{V})$. The duality map $< \cdot, \cdot >$ from $L^1(0,T;C(\mathcal{V})) \times R(0,T;\mathcal{V})$ to $\mathbb{R}$ will be defined by $< \mu, f >= \int_0^T \int_{\mathcal{V}} f(t) d\mu(t, dv) dt$ for all $f \in L^1(0,T;C(\mathcal{V}))$ and all $\mu \in R(0,T;\mathcal{V})$. A sequence μ_n in $R(0,T;\mathcal{V})$ is said to *weakly converge* to $\mu \in R(0,T;\mathcal{V})$ if

$$\lim_{n\to\infty} < \mu_n, f >= < \mu, f > \tag{8}$$

for all $f \in L^1(0,T;C(\mathcal{V}))$. Let $PC(0,T;\mathcal{D})$ denote the elements $\mu \in R(0,T;\mathcal{V})$ that are piecewise constant, and for each $t \in [0,T]$ the measure $\mu(t)$ is an element of the set of *Dirac measures* $\mathcal{D}$, that is, for each $t \in [0,T]$ there exists a $v \in \mathcal{V}$ such that the measure $\mu(t, \{v\})$ of $\{v\}$ is equal to 1. With these definitions, we can state and prove our next result.

Proposition IV.3: Given $T > 0$, let $\mathbf{y}(t)$ be the solution of the system (5) for some set of controls $\alpha_v : [0,T] \to [0,1]$ such that $\sum_{v\in\mathcal{V}} \alpha_v(t) = 1$ for all $t \in [0,T]$. Then, for each $\epsilon > 0$ there exists a control $\ell : [0,T] \to \mathcal{V}$ such that the solution $\mathbf{x}(t)$ of the system (3) satisfies $\|\mathbf{x}(T) - \mathbf{y}(T)\|_2 \le \epsilon$.

Proof: Let $\boldsymbol{\alpha} \in L^\infty(0,1;\mathcal{P}(\mathcal{V}))$ and let $\mu \in R(0,T;\mathcal{V})$ be the corresponding relaxed control. Then, from [17, Th. 12.6.7], there exists a sequence $(\mu_n)_{n=1}^\infty \in PC(0,T;\mathcal{D})$ that weakly converges to μ. Let $(\ell_n)_{n=1}^\infty$ be the sequence of piecewise constant functions from $[0,T]$ to $\mathcal{V}$ constructed by setting, for each $t \in [0,\infty)$ and each $v \in \mathcal{V}$, $\ell_n(t) = v$ if $\mu_n(t, \{v\}) = 1$. From [17], we know that solutions $\mathbf{z}_n(t)$ of the system (7) with relaxed control μ_n converge to the solution $\mathbf{z}$ of the system (7) with relaxed control μ, uniformly over the time interval $[0,T]$. ■

Lemma IV.2 states that trajectories of system (5) can be approximated arbitrarily well using trajectories of system (3). Combining Lemma IV.2 and Proposition IV.3, we obtain the following main theorem on *approximate controllability* of system (3), which gives an affirmative answer to a weaker form of Problem III.1 for which the state at the final time is only required to be within distance ϵ of the target final state.

Theorem IV.4: Let $\mathbf{x}^{eq} \in \operatorname{int} \mathcal{P}(\mathcal{V})$ be an equilibrium point of the system (5) with steady-state control input $\boldsymbol{\alpha}^{ss} = [\alpha_1^{ss} \dots \alpha_M^{ss}]^T \in \operatorname{int} \mathcal{P}(\mathcal{V})$. Additionally, let $T > 0$. Then there exists a neigborhood U of $\mathcal{P}(\mathcal{V})$, such that for each $\mathbf{x}^0 \in U$ and each $\epsilon > 0$, there exists a control $\ell : [0,T] \to \mathcal{V}$ such that the solution $\mathbf{x}(t)$ of the system (3) satisfies $\|\mathbf{x}(T) - \mathbf{x}^{eq}\|_2 \le \epsilon$.

Proof: According to Lemma IV.2, there exists a neighbourhood U of $\mathbf{x}^d$ such that if $\mathbf{x}^0 \in U$, then there exists a control $\boldsymbol{\alpha}(t)$ for the relaxed system (5) for which the solution $\mathbf{y}(t)$ satisfies $\mathbf{y}(T) = \mathbf{x}^{eq}$. It follows then from Proposition IV.3 that there exists a control $\ell(t)$ such that $\|\mathbf{x}(T) - \mathbf{x}^d\| = \|\mathbf{x}(T) - \mathbf{y}(T)\| \leq \epsilon$. ■

Remark IV.5: (Lack of Global Controllability) While Theorem IV.4 states that system (3) is locally approximately controllable about an equilibrium point $\mathbf{x}^{eq}$, in general, we cannot expect global controllability of the system for any $T > 0$. For example, consider the two-node bidirected graph $\mathcal{G}$ with $\mathcal{V} = \{1, 2\}$. Then, for a given positive parameter c, we set $u^0_{(1,2)}(\mathbf{y}) = cy_2^2$ and $u^0_{(2,1)}(\mathbf{y}) = cy_1^2$ for all $\mathbf{y} = [y_1\ y_2]^T \in [0, 1]^2$. If $x_1^0 < 0.5$ and $c > 0$ is large enough, then $\lim_{t\to 0^+} \dot{x}_1(t) < 0$ for any choice of piecewise constant $\ell(t)$. This implies that the system (3) is not controllable to the equilibrium point $\mathbf{x}^{eq} = [0.5\, 0.5]^T$ from $\mathbf{x}^0$ for any final time $T > 0$.

Remark IV.6: (Unbounded Speed of the Leader) It is important to note that in order to prove controllability of the system (3), we have implicitly assumed that the leader can switch between states arbitrarily fast. This implies that the leader can move at arbitrarily large speeds in space. However, in practice, the leader's speed will have an upper bound, which implies a lower bound on the switching times. This would, in turn, impose a lower bound on the parameter ϵ in Theorem IV.4 for which the approximate controllability result remains true. However, it is difficult to analytically quantify such a lower bound on ϵ as a function of a lower bound on the switching times.

V. Control Design and Stability Analysis

From here on, we will assume that the followers are not interacting with one another; that is, $u^0_e(\mathbf{x}) = 0$ for all $\mathbf{x} \in \mathcal{P}(\mathcal{V})$ and all $e \in \mathcal{E}$.

To address Problem III.2, we will construct two control laws that govern the leader's state transitions. Toward this end, we introduce some new definitions. A *complete walk*, denoted by $\mathcal{W} = (e_i)_{i=1}^w$, is a sequence of size $w \in \mathbb{Z}_{>0}$ in $\mathcal{E}$ such that $S(e_1) = T(e_w), T(e_i) = S(e_{i+1})$ for each $i \in \{1, \ldots, w-1\}$, and for each $v \in \mathcal{V}$ there exists $j \in \{1, \ldots, w\}$ such that $T(e_j) = v$. We will extend a given complete walk $\mathcal{W}$ to an *extended complete walk (ECW)*, $\mathcal{W}^\infty = (e_i)_{i=1}^\infty$, by defining

$$e_{nw+j} = e_j \text{ for } n \in \mathbb{Z}_{>0},\ j \in \{1, \ldots, w\}. \tag{9}$$

The sequence $\mathcal{W}^\infty$ denotes the path along which the leader can transition from one state to another.

A. Open-Loop Controller

We first construct an open-loop control strategy for the leader agent. An advantage of this control law over the feedback control law presented in Section V-B is that the leader is not required to measure the density of follower agents. Let $\mathbf{x}^{\text{eq}} \in \operatorname{int} \mathcal{P}(\mathcal{V})$, $\epsilon > 0$, and $t_0^\epsilon = 0$, and define

$$R_v = \{k \in \{1, \ldots, w\};\ S(e_k) = v\}.$$

We define switching times $(t_j^\epsilon)_{j=1}^\infty$ as

$$t_j^\epsilon = t_{j-1}^\epsilon + \frac{\epsilon}{|R_{S(e_j)}| x^{eq}_{S(e_j)}} \text{ for } j \in \mathbb{Z}_{>0} \tag{10}$$

where $|R_v|$ denotes the cardinality of the set R_v for each $v \in \mathcal{V}$. We also define $\ell^\epsilon : [0, \infty) \to \mathcal{V}$ as

$$\ell^\epsilon(t) = S(e_j) \text{ for } t \in [t_{j-1}^\epsilon, t_j^\epsilon),\ j \in \mathbb{Z}_{>0}. \tag{11}$$

Let $P = \sum_{k=1}^w t_k^1$ and

$$\mathbf{A}_{\text{av}} = \frac{1}{P} \int_0^P D_{\ell^1(t)} dt. \tag{12}$$

Then, setting $\tilde{\mathbf{A}} = \frac{1}{P} \sum_{v\in\mathcal{V}} \mathbf{D}_v$ and $\mathbf{D} = \operatorname{diag}[x_1^{\text{eq}} \ldots x_M^{\text{eq}}]^T$, we have that $\mathbf{A}_{\text{av}} = \tilde{\mathbf{A}}\mathbf{D}^{-1}$. Using these definitions, in the next result we establish that the solutions of system (3), for the choice of leader inputs (11), converge to solutions of a related time-varying system the time-invariant component of the dynamics (determined by the averaged matrix $\mathbf{A}_{av}$) is dominant.

Lemma V.1: Let $\ell(t) = \ell^\epsilon(t)$ in system (3). There exists $\epsilon_0 > 0$ and a time-varying matrix $\mathbf{A} : [0, \infty) \to \mathbb{R}^{M\times M}$ such that if $\epsilon \in (0, \epsilon_0]$, then the solution $\mathbf{x}(t)$ of (3) can be approximated using the solution $\mathbf{y}(t)$ of the equation

$$\dot{\mathbf{y}}(t) = \mathbf{A}_{\text{av}}\mathbf{y}(t) + \epsilon \mathbf{A}\left(\frac{t}{\epsilon}\right)\mathbf{y}(t),\ \ \mathbf{y}(0) = \mathbf{x}^0. \tag{13}$$

In particular, $\|\mathbf{x}(t) - \mathbf{y}(t)\| = O(\epsilon)$. Moreover, the map $t \mapsto \mathbf{A}(t)$ is such that the induced two-norm $\|\mathbf{A}(t)\|$ is globally bounded over $t \in \mathbb{R}_{\geq 0}$ and $\mathbf{A}(t + P) = \mathbf{A}(t)$ for all $t \in [0, \infty)$.

Proof: Consider the change of variables $\tau = \frac{t}{\epsilon}$. Then system (3) becomes

$$\dot{\mathbf{x}}(\tau) = \epsilon \mathbf{D}_{\ell(t)}\mathbf{x}(\tau). \tag{14}$$

Let $\mathbf{H}(\tau) = \mathbf{D}_{\ell(\tau)} - \mathbf{A}_{\text{av}}$ for each $\tau \in [0, \infty)$. Set $\mathbf{U}(\tau) = \int_0^\tau \mathbf{H}(s)ds$. Consider the change of variables

$$\mathbf{x}(\tau) = \mathbf{y}(\tau) + \epsilon \mathbf{U}(\tau)\mathbf{y}(\tau). \tag{15}$$

Then, we see that

$$\dot{\mathbf{x}}(\tau) = \dot{\mathbf{y}}(\tau) + \epsilon \mathbf{U}(\tau)\dot{\mathbf{y}}(\tau) + \epsilon \dot{\mathbf{U}}(\tau)\mathbf{y}(\tau). \tag{16}$$

For all ϵ small enough, $\mathbf{I} + \epsilon\mathbf{U}(\tau)$ is invertible for all $\tau \in [0, \infty)$ and can be represented by the power series expression

$$(\mathbf{I} + \epsilon \mathbf{U}(\tau))^{-1} = \sum_{i=0}^{\infty} (-\epsilon)^i \mathbf{U}^i(\tau). \tag{17}$$

From (14) and (17), and the fact that $\dot{\mathbf{U}}(\tau) = \mathbf{H}(\tau)$ and $\mathbf{D}_{\ell(\tau)} - \mathbf{H}(\tau) = \mathbf{A}_{\text{av}}$ for all $\tau \in [0, \infty)$, (16) can be used to solve for $\dot{\mathbf{y}}(\tau)$

$$\dot{\mathbf{y}}(\tau) = \epsilon \mathbf{A}_{\text{av}}\mathbf{y}(t) + \epsilon^2 \mathbf{A}(\tau)\mathbf{y}(\tau) \tag{18}$$

where $\mathbf{A}(\tau)$ is a time-varying matrix that is globally norm-bounded in time. From (15), and noting again that $\mathbf{I} + \epsilon\mathbf{U}(\tau)$ is invertible for all $\tau \in [0, \infty)$ for small enough ϵ, we conclude that $\|\mathbf{x}(t) - \mathbf{y}(t)\| = O(\epsilon)$ for all $t \geq 0$. The periodicity of $\mathbf{A}(\tau)$ follows from the fact that both $\mathbf{H}(\tau)$ and $\mathbf{U}(\tau)$ are periodic. ■

Using Lemma V.1, we can now establish the stability properties of system (3) with the control input $\ell(t) = \ell^\epsilon(t)$ defined

in (11). The following theorem uses the fact that solutions of system (13) can be used to approximate solutions of (3). The theorem applies an argument based on averaging theory [36] to prove *practical stability* of system (3).

Theorem V.2: Suppose the graph $\mathcal{G}$ is bidirected, $\mathcal{W}^\infty = (e_i)_{i=1}^\infty$ is an ECW, and $\mathbf{x}^{eq} \in \operatorname{int} \mathcal{P}(\mathcal{V})$. Let $\ell(t) = \ell^\epsilon(t)$. There exists $\epsilon_0 > 0$ such that for each $\epsilon \in (0, \epsilon_0]$, there exists $C_\epsilon \geq 0$ with $\lim_{\epsilon \to 0} C_\epsilon = 0$ and $T_\epsilon^{0,eq} > 0$, which depends on $\mathbf{x}^0$, $\mathbf{x}^{eq}$, and ϵ, such that $\|\mathbf{x}(t) - \mathbf{x}^{eq}\| < C_\epsilon$ for all $t \geq T_\epsilon^{0,eq}$.

Proof: Let $\mathbf{A} : [0, \infty) \to \mathbb{R}^{M \times M}$ be the time-varying matrix from Lemma V.1. Then consider the linear equation (13). Define a Lyapunov function $V : \mathcal{P}(\mathcal{V}) \to \mathbb{R}_{\geq 0}$ given by

$$V(\mathbf{z}) = (\mathbf{z} - \mathbf{x}^{\text{eq}})^T \mathbf{D} (\mathbf{z} - \mathbf{x}^{\text{eq}}) \tag{19}$$

for all $\mathbf{z} \in \mathcal{P}(\mathcal{V})$. Since the graph $\mathcal{G}$ is bidirected and strongly connected, we compute that

$$\frac{\partial V}{\partial \mathbf{y}}^T \mathbf{A}_{\text{av}} (\mathbf{y}(t) - \mathbf{x}^{\text{eq}}) = -\sum_{e \in \mathcal{E}} \frac{1}{2} (y_{S(e)}(t) - x^{\text{eq}}_{S(e)} - y_{T(e)}(t) + x^{\text{eq}}_{T(e)})^2 < 0$$

for all $t \geq 0$ such that $\mathbf{y}(t) \in \mathcal{P}(\mathcal{V}) \setminus \{\mathbf{x}^{\text{eq}}\}$. Then, we have that

$$\dot{V}(\mathbf{y}(t)) = \frac{\partial V(\mathbf{y}(t))}{\partial \mathbf{y}}^T \mathbf{A}_{\text{av}} (\mathbf{y}(t) - \mathbf{x}^{\text{eq}}) + \epsilon \frac{\partial V(\mathbf{y}(t))}{\partial \mathbf{y}}^T \mathbf{A}(t) \mathbf{y}(t). \tag{20}$$

since $\mathbf{A}_{\text{av}} \mathbf{x}^{\text{eq}} = \mathbf{0}$.

It follows from the computations in the proof of Lemma V.1 that all off-diagonal elements of $\mathbf{A}_{\text{av}} + \epsilon \mathbf{A}(\frac{t}{\epsilon})$ are nonnegative and that

$$\mathbf{1}^T \left(\mathbf{A}_{\text{av}} + \epsilon \mathbf{A} \left(\frac{t}{\epsilon} \right) \right) = \mathbf{0}$$

for all $t \in [0, \infty)$ and for all $\epsilon > 0$ small enough. Here, we are using the fact that the matrix $\mathbf{U}(\tau)$ constructed in the proof of Lemma V.1 can have a nonzero value at its ijth entry only if $\mathbf{A}_{\text{av}}$ has a nonzero value at its ijth entry. Then, from Lemma V.1 and Remark III.3, we can conclude that $\mathcal{P}(\mathcal{V})$ is invariant for the solution $\mathbf{y}(t)$. Since $\mathcal{P}(\mathcal{V})$ is a compact set, this result implies that the term $\frac{\partial V(\mathbf{y}(t))}{\partial \mathbf{y}}^T \mathbf{A}(t) \mathbf{y}(t)$ is uniformly bounded. Thus, the second term in the right-hand side of equation (20) is bounded by the parameter

$$C'_\epsilon = \epsilon \sup_{\mathbf{y} \in \mathcal{P}(\mathcal{V})} \left| \frac{\partial V}{\partial \mathbf{y}} \right| \sup_{t \in [0,T]} \|\mathbf{A}(t)\|$$

for each $\epsilon > 0$, and we have that $\lim_{\epsilon \to 0} C'_\epsilon = 0$. This implies that for all $\epsilon > 0$ small enough, $\dot{V}(\mathbf{y}(t)) < 0$ for all $t \in [0, \infty)$ such that $\|\mathbf{y}(t) - \mathbf{x}^{eq}\| > C_\epsilon$, where $C_\epsilon \to 0$ as $\epsilon \to 0$. In turn, this implies that $V(\mathbf{y}(t))$ is strictly decreasing whenever $\|\mathbf{y}(t) - \mathbf{x}^{eq}\| > C_\epsilon$. Hence, for all t that are sufficient large, $\|\mathbf{y}(t) - \mathbf{x}^{eq}\| \leq C_\epsilon$. ■

Remark V.3: (Extension to Strongly Connected Graphs) The assumption that the graph $\mathcal{G}$ is bidirected has been made for the sake of simplicity. Theorem V.2 can be generalized to strongly connected graphs that are not necessarily bidirected by replacing $\frac{\epsilon}{|R_{S(e_j)}| x^{\text{eq}}_{S(e_j)}}$ with $\frac{\epsilon x^d_{S(e_j)}}{|R_{S(e_j)}| x^{\text{eq}}_{S(e_j)}}$ in (10) for each $j \in \mathbb{Z}_{>0}$, where, from the Perron–Frobenius theorem [3], $\mathbf{x}^d$ is the unique vector in $\mathcal{P}(\mathcal{V})$ such that $\sum_{e \in \mathcal{E}} \mathbf{B}_e \mathbf{x}^d = \mathbf{0}$.

B. Closed-Loop Controller

In contrast to the open-loop control law presented in the previous section, the control law that we present in this section is a function of the density of the followers at the leader's current state. We show through numerical simulations in Section VI that this closed-loop controller ensures faster convergence of the followers to the target distribution than the open-loop controller.

Given $\mathbf{x}^{\text{eq}} \in \mathbb{R}^M$, we define the set $\mathcal{Q} \subset \mathbb{R}^M \times \mathbb{Z}_{>0}$ as

$$\mathcal{Q} = \{(\mathbf{x}, k) \in \mathbb{R}^M \times \mathbb{Z}_{>0};\ x_{S(e_k)} \leq x^{\text{eq}}_{S(e_k)}\}. \tag{21}$$

The set $\mathcal{Q}$ is used as follows to define the feedback control law according to which the leader transitions from one state to another. If the leader is in state $S(e_k)$ and the density of follower agents in that state, $x_{S(e_k)}$, is less than or equal to the target value $x^{\text{eq}}_{S(e_k)}$, then the leader transitions to the next state $T(e_k)$ in $\mathcal{W}^\infty$. While the path that the leader takes is predetermined by the specification of $\mathcal{W}^\infty$, the times at which it switches from one state to another is a function of the follower density that it measures at its current state, according to the following equations:

$$\begin{aligned} k(t^+) &= k(t^-) + 1 \\ \ell(t^+) &= T(e_{k(t^-)}),\ (\mathbf{x}(t^-), k(t^-)) \in \mathcal{Q} \end{aligned} \tag{22}$$

where $k(t^+)$ and $\ell(t^+)$ denote the right-sided limits of the functions $k(t)$ and $\ell(t)$, respectively, at time t, and $k(t^-)$ and $\ell(t^-)$ denote the left-sided limits of $k(t)$ and $\ell(t)$ at t. This control law for the leader, combined with the ODE model (3) that governs the follower agent densities, results in a *hybrid dynamical system* [18] in which the continuous-time dynamics are given by the following.

$$\begin{aligned} \dot{\mathbf{x}}(t) &= \mathbf{D}_{\ell(t)} \mathbf{x}(t) \\ \dot{k}(t) &= 0 \\ \dot{\ell}(t) &= 0, \quad t \in [0, \infty) \end{aligned} \tag{23}$$

the discrete-time dynamics are given by (22), and the initial conditions are defined as follows:

$$\mathbf{x}(0) = \mathbf{x}^0 \in \mathcal{P}(\mathcal{V}),\ \ k(0) = 0,\ \ \ell(0) = S(e_1). \tag{24}$$

Algorithm 1 presents a pseudocode that simulates the motion of a leader agent governed by control law (22) and the motion of N follower agents that respond to the leader's presence according to the dynamics (3).

Since the closed-loop system (22)–(24) is a hybrid system, we need an appropriate notion of a solution to this type of system in order to establish our stability result in Theorem V.8. Hence, we provide the following definition that will be sufficient for the purposes of this article.

Definition V.4: Suppose that $\mathcal{W}^\infty = (e_i)_{i=1}^\infty$ is a given ECW. By a solution of the system (23) and (24), we mean that there

Algorithm 1: Simulation of Closed-Loop System.

Inputs: $\Delta t, t_f, \mathcal{G} = (\mathcal{V}, \mathcal{E}), \mathcal{W}^\infty = (e_1, e_2, \ldots), N$
Initialize $n = 1, t = 0, \ell(0) = S(e_1), X_j(0) \in \mathcal{V}$
while $t < t_f$ **do**
  while $\frac{1}{N}\sum_{j=1}^{N} \chi_{\ell(t)}(X_j(t)) > x^{eq}_{\ell(t)}$ **do**
    for $j = 1$ to N **do**
      if $X_j(t) = \ell(t)$ **then** $X_j(t + \Delta t) = w$ for $w \in \mathcal{N}(\ell(t))$ with probability $\eta \Delta t$,
      end if
    end for
    $t = t + \Delta t$
  end while
  $n = n + 1$
  $t_n = t$
  $\ell(t_n) = T(e_n)$ ▷Leader jumps to next state
end while

exists a time $t_f \geq 0$ (possibly equal to ∞), an absolutely continuous function $\mathbf{x} : [0, t_f) \to \mathcal{P}(\mathcal{V})$, piecewise constant functions $k : [0, t_f) \to \mathbb{Z}_{>0}$ and $v_l : [0, t_f) \to \mathcal{V}$, and a sequence of nondecreasing switching times $(t_i)_{i=1}^{\infty}$ such that $\lim_{j\to\infty} t_j = t_f$ and, for each $i \in \mathbb{Z}_{>0}$, we have that

$$\mathbf{x}(t) = \mathbf{x}_0 + \int_0^{\min\{t,t_i\}} \mathbf{D}_{\ell(t)}\mathbf{x}(\tau)d\tau \tag{25}$$

and

$$\begin{aligned} &k(t) = i, \quad t \in [t_{i-1}, t_i),\ (\mathbf{x}(t_i), k(t_i)) \in \mathcal{Q} \\ &\ell(t) = T(e_{i-1}),\ t \in [t_{i-1}, t_i) \end{aligned} \tag{26}$$

where $t_0 = 0$ and $[t_{i-1}, t_i) := \emptyset$ is the null set if $t_{i-1} = t_i$.

Given this definition, we prove the following result on the existence and uniqueness of solutions of the system (23) and (24). In the following theorem and henceforth, $\operatorname{int}\mathcal{P}(\mathcal{V})$ will denote the interior of the set $\mathcal{P}(\mathcal{V})$ in the subspace topology of $\mathcal{P}(\mathcal{V})$ as a subset of $\mathbb{R}^M$.

Theorem V.5: Suppose that $\mathcal{W}^\infty = (e_i)_{i=1}^{\infty}$ is an ECW and $\mathbf{x}^{eq} \in \operatorname{int}\mathcal{P}(\mathcal{V})$. Then there exists a unique solution to the system (22)–(24) with switching times $(t_i)_{i=1}^{\infty}$.

Proof: The strategy of the proof is the following. We can exactly compute the first nonzero switching time as a function of the initial leader position and the follower distribution. Between each of the computed switching times, the system (22)–(24) is a linear system. Therefore, we will start by constructing a *local solution* from $t_0 = 0$ until the first nonzero switching time using the exponential of a matrix. Then, we will iteratively construct a global solution from this local solution.

First, we show that there at least exists a unique *local solution* of system (23) and (24). Specifically, we show that there exists $j \in \mathbb{Z}_{>0}$ and a sequence of switching times $(t_i)_{i=1}^{j}$ such that $\mathbf{x} : [0, t_j] \to \mathcal{P}(\mathcal{V})$ is absolutely continuous and equations (25) and (26) hold for each $i \in \{1, \ldots, j\}$. Let i_1, defined as

$$i_1 = \min\{m \in \mathbb{Z}_{>0};\ x_{S(e_m)}(0) > x^{\text{eq}}_{S(e_m)}\}$$

be the index of the first switching time at which the leader is at a state where the distribution of the followers is greater than the target distribution. If i_1 does not exist, then the initial distribution of the followers is less than or equal to the target distribution, and we set $t_i = 0$ for all $i \in \mathbb{Z}_{>0}$. In this case, the existence of a unique local solution is trivial. Alternatively, suppose that i_1 is finite; that is, there exists at least one state along the leader's trajectory where the current follower distribution is higher than the target distribution. Let $t_i = 0$ for all $i \in \{\tilde{i} \in \mathbb{Z}_{>0};\ 0 < \tilde{i} < i_1\}$. Set $v = S(e_{i_1})$ and

$$t_{i_1} = \frac{1}{|\mathcal{N}(S(v))|} \ln \frac{x_v(0)}{x_v^{\text{eq}}}.$$

Note that v is the first state at which the leader spends a nonzero amount of time, which is equal to t_{i_1}. Since $\mathbf{x}^{\text{eq}}$ lies in the interior of $\mathcal{P}(\mathcal{V})$, the quantity $\ln \frac{x_v(0)}{x_v^{eq}}$ is well-defined. It follows that:

$$\dot{x}_v(s) = -|\mathcal{N}(v)| x_v(s)$$

for all $s \in [0, t_{i_1})$. This implies that

$$x_v(s) = e^{-|\mathcal{N}(v)|s} x_v(0)$$

for all $s \in [0, t_{i_1})$, and hence $\lim_{s\to t_{i_1}} x_v(s) = x_v^{eq}$. Then, we set $k(t) = i_1$ and $\ell(t) = v$ for all $t \in [0, t_{i_1})$. Thus, we have established that at least one local solution of system (22)–(24) exists. This constructed local solution can be nonunique only if there is an alternative possible choice of switching times, $(\tilde{t}_i)_{i=1}^{\tilde{j}}$. This alternative set of switching times is valid only if the first nonzero switching time is chosen to have an index greater than i_1. However, this would violate the requirement in constraint (26) that $(\mathbf{x}(t_i), k(t_i)) \in \mathcal{Q}$. Hence, the constructed local solution is unique.

Next, we will show that any local solution can be extended to a unique *global solution* that is defined over a countably infinite sequence of switching times. Suppose there exists a unique local solution of system (23) and (24). That is, there exists $p \in \mathbb{Z}_{>0}$, possibly larger than i_1, and a sequence of switching times such that $\mathbf{x} : [0, t_p] \to \mathcal{P}(\mathcal{V})$ is absolutely continuous and equations (25) and (26) hold for each $i \in \{1, \ldots, p\}$. Let q_1, defined as

$$q_1 = \min\{m \in \mathbb{Z}_{>0};\ m > p \lim_{t\to t_p} x_{S(e_m)}(t) > x^{\text{eq}}_{S(e_m)}\}$$

be the index of the first switching time after p at which the leader is at a state where the distribution of followers is greater than the target distribution. If q_1 does not exist, then we set $t_i = t_p$ for all $i \in \mathbb{Z}_+$ such that $i \geq p$, and the existence of a unique global solution is trivial. Alternatively, suppose that q_1 is finite. Let $t_i = t_p$ for all $i \in \{\tilde{i} \in \mathbb{Z}_{>0};\ p < \tilde{i} < q_1\}$. Set $v = S(e_{q_1})$ and

$$t_{q_1} = t_p + \frac{1}{|\mathcal{N}(S(v))|} \ln \frac{x_v(t_p)}{x_v^{eq}}.$$

Then, we can see that

$$\dot{x}_v(s) = -|\mathcal{N}(v)| x_v(s)$$

for all $s \in [t_{q_1-1}, t_{q_1})$. This implies that

$$x_v(s) = e^{-|\mathcal{N}(v)|(s - t_{q_1-1})} x_v(t_{q_1-1})$$

for all $s \in [t_{q_1-1}, t_{q_1})$, and hence that $\lim_{s\to t_{q_1}} x_v(s) = x_v^{\text{eq}}$. Then, we set $k(t) = q_1$ and $\ell(t) = v$ for all $t \in [t_{q_1-1}, t_{q_1})$.

Therefore, any local solution can be extended uniquely over a longer time interval. Since, we have already constructed one such local solution, this implies that we can iteratively construct a unique global solution $\mathbf{x}$ to system (22)–(24) by extending each local solution to another local solution over successively longer time intervals. Because this solution is both continuous and piecewise continuously differentiable, and therefore Lipschitz, it is absolutely continuous. ■

In the next lemma, we derive an estimate of the solutions of system (22)–(24) that will be used to prove the main asymptotic stability result stated in Theorem V.8.

Lemma V.6: Suppose that $\mathbf{x}^{\text{eq}} \in \operatorname{int} \mathcal{P}(\mathcal{V})$. Let there exist some $j \in \mathbb{Z}_{>0}$ and $\epsilon > 0$ such that the solution of system (22)–(24) satisfies $x_v(t_{j-1}) > x_v^{\text{eq}} + \epsilon$ for $v = S(e_j)$. Then

$$x_w(t_j) > x_w(t_{j-1}) + \frac{\epsilon}{|\mathcal{N}(v)|}$$

for all $w \in \mathcal{N}(v)$.

Proof: By assumption, we have that

$$x_v(t_{j-1}) > x_v^{\text{eq}} + \epsilon$$

for $v = S(e_j)$. Then

$$t_j = t_{j-1} + \frac{1}{|\mathcal{N}(v)|} \ln \frac{x_v(t_{j-1})}{x_v^{\text{eq}}}.$$

This implies that $\dot{x}_v(t) = |\mathcal{N}(v)| x_v(t)$ and $\dot{x}_w(t) = -x_v(t)$ for all $t \in [t_{j-1}, t_j)$ and all $w \in \mathcal{N}(v)$. Therefore

$$x_w(t_j) = x_w(t_{j-1}) + \frac{x_v(t_{j-1}) - x_v^{\text{eq}}}{|\mathcal{N}(v)|}$$

for all $w \in \mathcal{N}(v)$. ■

The following proposition establishes an important monotonicity property of solutions of system (22)–(24) that is used in the proof of Theorem V.8, which states the main asymptotic stability result.

Proposition V.7: Suppose there exist times $\tau_1 > 0$, $\tau_2 > \tau_1$ and state $v \in \mathcal{V}$ such that the solution $\mathbf{x}(t)$ of system (22)–(24) satisfies $x_v(t) \leq x_v^{eq}$ for all $t \in [\tau_1, \tau_2]$. Then, $x_v(t)$ is nondecreasing over the interval $t \in [\tau_1, \tau_2]$. Hence, if there exist $\tilde{\tau} \geq 0$ and $w \in \mathcal{V}$ such that the solution $\mathbf{x}(t)$ satisfies $x_w(\tilde{\tau}) \geq x_v^{eq}$, then $x_w(t) \geq x_v^{eq}$ for all $t \in [\tilde{\tau}, t_f)$.

Proof: We are given that $x_v(t) \leq x_v^{eq}$ for all $t \in [\tau_1, \tau_2]$. Hence, $t_k - t_{k-1} = 0$ for all $k \in \mathbb{Z}_+$ such that $v = S(e_k)$ and $t_k \in [\tau_1, \tau_2]$. Moreover, $\dot{x}_v(t) \geq 0$ for all $t \in [t_{k-1}, t_k)$, since $g_{e_k}(\ell(t)) = 0$ whenever $v \neq S(e_k)$. This implies that $\dot{x}_v(t) \geq 0$ for $t \in (\tau_1, \tau_2)$, and therefore $\int_{\tau_1}^{t} \dot{x}_v(s) ds$ is nondecreasing for $t \in [\tau_1, \tau_2]$. Since the solution $\mathbf{x}$ is absolutely continuous, we have that

$$x_v(t) - x_v(\tau_1) = \int_{\tau_1}^{t} \dot{x}_v(s) ds$$

for all $t \in [\tau_1, \tau_2]$. ■

The result proved in Proposition V.7 can be used to demonstrate that the target probability distribution $\mathbf{x}^{\text{eq}}$ is stable in the sense of Lyapunov. In the following theorem, we establish that this distribution is also globally attractive.

Theorem V.8: Suppose that $\mathcal{W}^{\infty} = (e_i)_{i=1}^{\infty}$ is an ECW and $\mathbf{x}^{eq} \in \operatorname{int} \mathcal{P}(\mathcal{V})$. Then, the unique solution of system (22)–(24) satisfies

$$\lim_{t \to t_f} \mathbf{x}(t) = \mathbf{x}^{\text{eq}}.$$

Proof: We proves this result by contradiction. Suppose that $\lim_{i \to \infty} \mathbf{x}(t_i) \neq \mathbf{x}^{\text{eq}}$. Then, there must be a $v \in \mathcal{V}$ and $\epsilon > 0$ such that for each $N \in \mathbb{Z}_{>0}$, there exists $p_N \geq N$ for which $x_v(t_{p_N - 1}) > x_v^{\text{eq}} + \epsilon$. From Lemma V.6, this implies that for every $w \in \mathcal{N}(v)$,

$$x_w(t_{p_N}) > x_w(t_{p_N - 1}) + \frac{\epsilon}{|\mathcal{N}(v)|}.$$

Because $\epsilon > 0$, it follows that there exists an $M \in \mathbb{Z}_{>0}$ that satisfies

$$\frac{M\epsilon}{|\mathcal{N}(v)|} \geq x_v^{\text{eq}}$$

and hence Proposition V.7 implies that

$$x_w(t) \geq x_w^{\text{eq}} + \frac{\epsilon}{|\mathcal{N}(v)|}$$

for $t = t_{p_{M+1}}$ for all $w \in \mathcal{N}(v)$. Since the graph $\mathcal{G}$ is assumed to be strongly connected, Lemma V.6 also implies that for each $r \in \mathcal{V}$, there exists $\tilde{\epsilon}_r > 0$ and $q_N^r \in \mathbb{Z}_+$ corresponding to each $N \in \mathbb{Z}_{>0}$ such that $x_r(t) \geq x_r^{\text{eq}} + \tilde{\epsilon}_r$ for $t = t_z$ with $z = q_N^r$. Due to the monotonicity result in Proposition V.7, this implies that $x_r(t) \geq x_r^{\text{eq}}$ for all $r \in \mathcal{V}$ for all sufficiently large times t. This implies that $\sum_{v \in \mathcal{V}} x_v(t) > 1$ for some time $t \in [0, \infty)$. This leads to a contradiction with the fact that the set $\mathcal{P}(\mathcal{V})$ is invariant for the solution $\mathbf{x}(t)$. Hence, it must be true that $\lim_{i \to \infty} \mathbf{x}(t_i) = \mathbf{x}^{\text{eq}}$. From the monotonicity property of solutions proved in Proposition V.7, it follows that $\lim_{t \to t_f} \mathbf{x}(t) = \mathbf{x}^{\text{eq}}$. ■

Remark V.9: (*Zeno Behavior*) Note that it is possible that $\lim_{i \to \infty} t_i = t_f < \infty$. In fact, this is trivially true when $\mathbf{x}(0) = \mathbf{x}^{eq} \in \operatorname{int} \mathcal{P}(\mathcal{V})$.

Remark V.10: (Stabilizing a Swarm of Interacting Robots) Stabilization of the followers to a target probability distribution required the assumption that the followers are not interacting. While this assumption is not required for the open-loop controller that was studied in Section V-A, significantly more work would be needed to extend the closed-loop controller introduced in this section to the case of interacting followers. First, following Remark IV.5, we cannot ensure global stability of the target distribution. Second, it cannot be guaranteed that the monotonicity property of the solutions that was established in Proposition V.7 would still hold if the followers were interacting. One possible approach to designing a local stabilizing controller for the case of interacting agents is similar to the approach we used to prove local approximate controllability of the system (3): construct a stabilizing controller for the relaxed system (5) and then construct a switching controller that mimics the behavior of the controller for the relaxed system and locally approximately stabilizes the original system (3).

We note that the number of switchings in the control laws presented in this section and in Section V-A depends on the

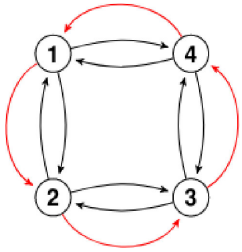

Fig. 2. Bidirected graph with four vertices, representing agent states. Red edges define the leader's sequence of state transitions; black edges define followers' possible state transitions.

number of possible states of a single follower agent. In many applications, the actual state space of each follower agent would be continuous, and the state space of the corresponding Markov chain that models the motion of each agent would be obtained by discretizing this continuous state space. Therefore, as the state space of the Markov chain converges to the actual continuous state space of the followers, the control law presented in this section would require an increasing amount of time to drive the followers to the target distribution. This contrasts with the control approach presented in [25], in which the state space of each follower agent is continuous, and hence no discretization of the state space is required in the modeling process. However, the control approach in [25] does not scale well with the number of follower agents, since the leader must have the ability to distinguish between the followers and switch successively between them. For potential applications such as artificial pollination by robotic insects [5], where the number of agents is expected to be on the order of thousands, it may be sufficient to prescribe the target swarm behavior in terms of desired probability distributions of agents or agent activity on a coarse discretization of the agents' state space, thus making the herding approach presented in this article more appropriate. On the other hand, in applications, where the number of followers is small and the goal is to control them to precise locations in space, the approach in [25] might be more suitable.

VI. Numerical Simulations

In this section, we verify the effectiveness of our control strategies with numerical simulations in MATLAB of three scenarios with different controllers, graph topologies, and follower agent population sizes. In the first scenario, the leader agent must herd the follower agents to a target distribution over an undirected four-vertex grid graph with the topology shown in Fig. 2. The leader moves along the path $\mathcal{W}^\infty = ((1,2),(2,3),(3,4),(4,1),(1,2),\ldots)$. The initial distribution of followers was set to $\mathbf{x}^0 = [1\ 0\ 0\ 0]^T$, and the target distribution was defined as $\mathbf{x}^{\text{eq}} = [0.1\ 0.1\ 0.4\ 0.4]^T$. Fig. 3(a) and (b) compares the solution of the system (3) to the stochastic simulation of the CTMC characterized by expression (1) with the open-loop controller (11) for two different follower population sizes, $N = 20$ and $N = 200$, with the corresponding switching parameter value set to $\epsilon = 0.05$ and $\epsilon = 0.01$, respectively. As expected, the plots show that the stochastic simulation for the $N = 200$ case follows the mean-field model solution more closely than for the $N = 20$ case. In both cases, the difference between the average follower populations and the target distributions converges to 0 within 27.5 s. For the $N = 20$ case, in which $\epsilon = 0.05$, the solution of the mean-field model shows larger fluctuations about the target distribution than for the $N = 200$ case, in which $\epsilon = 0.01$. This is consistent with the result in Theorem V.2 that decreasing the value of ϵ produces smaller fluctuations of the solution of the mean-field model about the target distribution as $t \to \infty$.

In the second scenario, the graph topology and the path of the leader are the same as in the first scenario. The initial distribution of followers was set to $\mathbf{x}^0 = [1\ 0\ 0\ 0]^T$, and the target distribution was defined as $\mathbf{x}^{\text{eq}} = [0.25\ 0.25\ 0.25\ 0.25]^T$. Fig. 3(c) and (d) compare the solution of system (3) to a stochastic simulation of the CTMC characterized by expression (1) with the closed-loop controller (22) for two different follower population sizes, $N = 20$ and $N = 200$. As expected, the plots show that the stochastic simulation for the $N = 200$ case follows the mean-field model solution more closely than for the $N = 20$ case. In both cases, the average follower populations converge to the target distribution within 3.5 s. Compared to the open-loop controller used in the first scenario, we observe that the closed-loop controller achieves much faster convergence of the swarm to the target distribution.

To demonstrate the scalability of our control approach, we considered two scenarios in which the leader must herd $N = 10^4$ follower agents to a target distribution over a 36-vertex graph (*Scenario 1*) and a 100-vertex graph (*Scenario 2*). Both graphs are bidirected and have a 2-D grid structure. For both scenarios, all the follower agents start in a single state (the bottom left grid cell), and the transition rate η is set to $\eta = 1$. *Scenario 1:* One-tenth of the follower agents are required to distribute equally among the boundary cells and four cells at the center, while nine-tenths of the population is required to distribute equally among the remaining cells to form the letter "O." Fig. 4 shows snapshots at times $t = 0$ s, $t = 100$ s, and $t = 1000$ s of the distribution of follower agents and location of the leader agent in a stochastic simulation of the CTMC characterized by expression (1) with the closed-loop controller (22). Let $N_v(t)$ denote the number of follower agents in state $v \in \mathcal{V}$ at time t in the stochastic simulation, and define $\mathbf{x}^s(t) = \frac{1}{N}[N_1(t) \ldots N_{36}(t)]^T$ as the vector of followers' population fractions in different states at time t. Measuring the difference between the simulated and target distributions of follower agents at time t as the error $E(t) = ||\mathbf{x}^s(t) - \mathbf{x}^{\text{eq}}||_2$, we compute $E(0) = 1.04$, $E(40) = 3.9 \times 10^{-2}$, and $E(400) = 1.4 \times 10^{-3}$ for the times of the snapshots in Fig. 4. The decreasing value of $E(t)$ over time indicates that the follower agent distribution converges to the target distribution as desired, which can also be confirmed qualitatively from the snapshots. A movie of the numerical simulation with the closed-loop controller is shown in the video attachment. *Scenario 2:* The follower agents are required to distribute on the 100-vertex graph to form the letters "ASU." Ninety percent of the agents must distribute equally among cells that form the letters, and 10 % must distribute equally among the remaining cells. Fig. 5 shows snapshots at times $t = 0$ s,

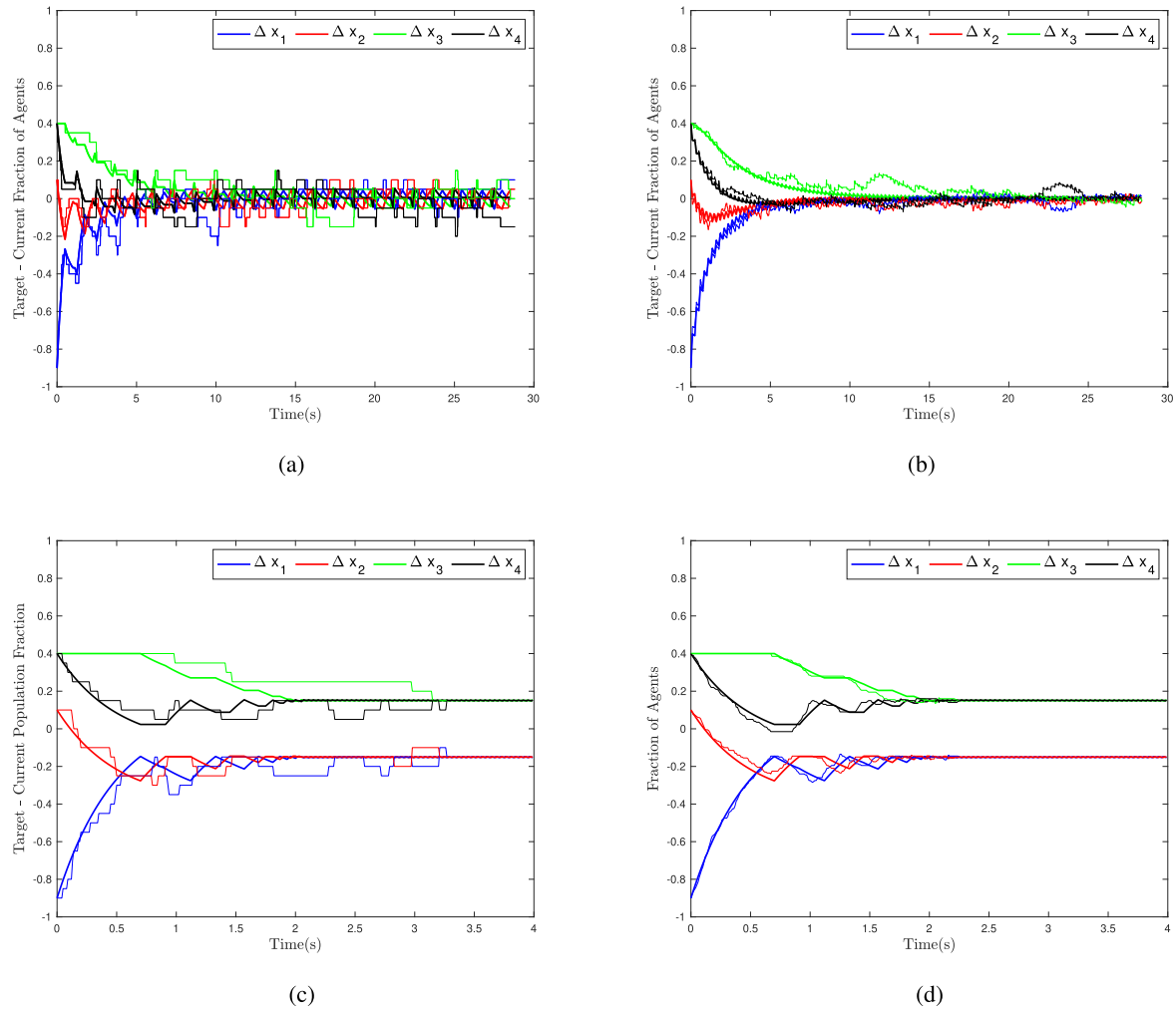

Fig. 3. Trajectories of the mean-field model *(thick lines)* and the corresponding stochastic simulations *(thin lines)*. (a) Open-loop control with $N = 20$ follower agents ($\epsilon = 0.05$. (b) Open-loop control with $N = 200$ follower agents ($\epsilon = 0.01$. (c) Closed-loop control with $N = 20$ follower agents. (d) Closed-loop control with $N = 200$ follower agents.

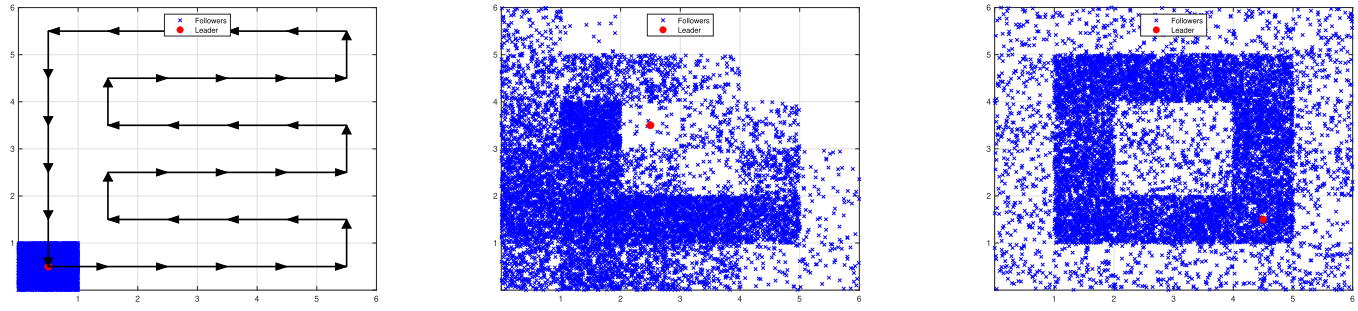

Fig. 4. Snapshots at three times t of $N = 10^4$ follower agents redistributing over a 36-vertex graph during a stochastic simulation of the closed-loop system. The black arrows define the sequence of state transitions by the leader agent. (a) $t = 0$ s. (b) $t = 40$ s. (c) $t = 400$ s.

$t = 300$ s, and $t = 3000$ s of the distribution of follower agents and location of the leader agent in a stochastic simulation of the CTMC characterized by expression (1) with the closed-loop controller (22). As expected, since the number of states for the 100-vertex graph is greater than for the 36-vertex graph, the agents take longer to converge to the target distribution on the 100-vertex graph. We compute the error $E(t)$ at the times t of the snapshots in Fig. 5 as $E(0) = 1.02$, $E(300) = 1.7 \times 10^{-2}$, and $E(3000) = 7.9 \times 10^{-4}$. As in *Scenario 1*, the decrease in $E(t)$ over time indicates that the follower distribution converges to the target distribution, which can also be confirmed qualitatively from the snapshots.

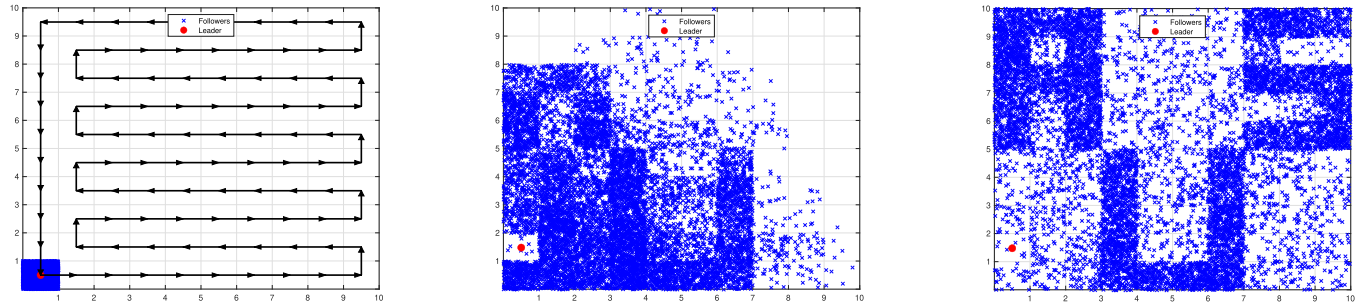

Fig. 5. Snapshots at three times t of $N = 10^4$ follower agents redistributing over a 100-vertex graph during a stochastic simulation of the closed-loop system. The black arrows define the sequence of state transitions by the leader agent. (a) $t = 0$ s. (b) $t = 300$. (c) $t = 3000$.

TABLE I
EFFECT OF VARIATIONS IN FOLLOWER TRANSITION RATE OR LEADER MEASUREMENT ACCURACY ON ERROR $E(400)$ IN *SCENARIO 1*

$\Delta\eta$	$E(400)$
$+0.50$	8.8×10^{-3}
$+0.25$	4.6×10^{-3}
0	1.4×10^{-3}
-0.25	2.2×10^{-3}
-0.50	8.3×10^{-3}

ΔK	$E(400)$
$+0.50$	6.0×10^{-3}
$+0.25$	5.7×10^{-3}
0	1.4×10^{-3}
-0.25	2.2×10^{-3}
-0.50	2.0×10^{-3}

TABLE II
EFFECT OF VARIATIONS IN FOLLOWER TRANSITION RATE OR LEADER MEASUREMENT ACCURACY ON ERROR $E(3000)$ IN *SCENARIO 2*

$\Delta\eta$	$E(3000)$
$+0.50$	2.7×10^{-3}
$+0.25$	1.1×10^{-3}
0	7.9×10^{-4}
-0.25	1.5×10^{-3}
-0.50	2.2×10^{-3}

ΔK	$E(3000)$
$+0.50$	1.3×10^{-3}
$+0.25$	9.5×10^{-4}
0	7.9×10^{-4}
-0.25	1.5×10^{-3}
-0.50	1.8×10^{-3}

Additional numerical simulations of *Scenario 1* and *Scenario 2* were performed to investigate the robustness of the closed-loop controller to (a) variations in the transition rate η, the rate at which follower agents exit their state due to the leader's presence; and (b) inaccuracy in the leader's estimate of the fraction of follower agents at its current location. For simulations of case (a), the leader obtained accurate measurements of the follower population, and the transition rate η was set to $\eta = 1 + \Delta\eta$, $\Delta\eta \in \{0.5, 0.25, 0, -0.25, -0.5\}$. The parameter $\Delta\eta = 0$ corresponds to the nominal scenario where $\eta = 1$. For simulations of case (b), η was fixed at $\eta = 1$, and the leader's estimate of the empirical distribution $\frac{1}{N}\sum_{i=1}^{N} \chi_v(X_i(t))$ was modeled as $\frac{1}{N}\sum_{i=1}^{N} \chi_v(X_i(t))(1 + \Delta K Y_v(t))$ for $\Delta K \in \{0.5, 0.25, 0, -0.25, -0.5\}$, where $Y_v(t) \in [0, 1]$ is a uniform random variable. The parameter $\Delta K = 0$ corresponds to the scenario where the leader's estimate is accurate. Tables I and II list the values of the error $E(t)$ computed at the final time of the simulations of *Scenario 1* and *Scenario 2*, respectively, for both cases (a) and (b). The minimum error values are achieved for the nominal value of η ($\Delta\eta = 0$) and accurate leader measurements ($\Delta K = 0$). However, relatively low error values are still obtained when $\Delta\eta \neq 0$ and $\Delta K \neq 0$, indicating that the closed-loop controller is able to successfully drive the follower agents close to the target distribution even in the presence of variations in η and inaccuracy in the leader's measurements.

VII. PHYSICAL ROBOT EXPERIMENTS

Three multirobot experiments were implemented using the *Robotarium* [31] to validate the closed-loop controller (22). The Robotarium is a swarm robotics testbed that users can remotely access to validate their controllers and algorithms on physical hardware. The experiment was conducted in a centralized manner, in that the robot population in each state was measured from images taken from multiple VICON motion capture cameras, and the robots initiated and completed their transitions between states when commanded by a central computer.

In Experiment 1, the environment was modeled as an undirected four-vertex grid graph $\mathcal{G}$ and $N = 10$ robots were used as follower agents. The robots move on the testbed surface shown in Fig. 6(a), which is divided into four regions of equal size, each of which corresponds to a vertex of the graph $\mathcal{G}$ (superimposed on the testbed). A virtual leader agent, shown as the blue circle in Fig. 6(b), and the boundaries of the four regions were projected onto the testbed using an overhead projector. The initial and target follower agent distributions were defined as $N\mathbf{x}^0 = [4\,1\,1\,4]^T$ and $N\mathbf{x}^{\text{eq}} = [1\,4\,4\,1]^T$, respectively. The leader moves along the path $\mathcal{W}^\infty = [(1,2),(2,4),(4,3),(3,1),(1,2),\ldots]$. The leader remains stationary in its current state, repelling followers in that state, until the follower population in the leader's state is less than or equal to the target population; then, the leader transitions to the next state in its path. The leader was able to herd the robots into the target distribution in 20 iterations, as shown in Fig. 7(a), which plots the difference between the target distribution and current population in each state over time. In Experiment 2, the environment was the same as in Experiment 1 and $N = 18$ robots were used. The initial and target follower agent distributions were defined as $N\mathbf{x}^0 = [6\,3\,3\,6]^T$ and $N\mathbf{x}^{\text{eq}} = [3\,6\,6\,3]^T$, respectively. The leader was able to herd the robots into the target distribution in 15 iterations, as shown in Fig. 7(b). In Experiment 3, the environment was modeled as an undirected six-vertex grid graph $\mathcal{G}$, and $N = 12$ robots were used as follower agents. The robots move on the testbed surface shown in Fig. 6(b), which is divided into six regions of

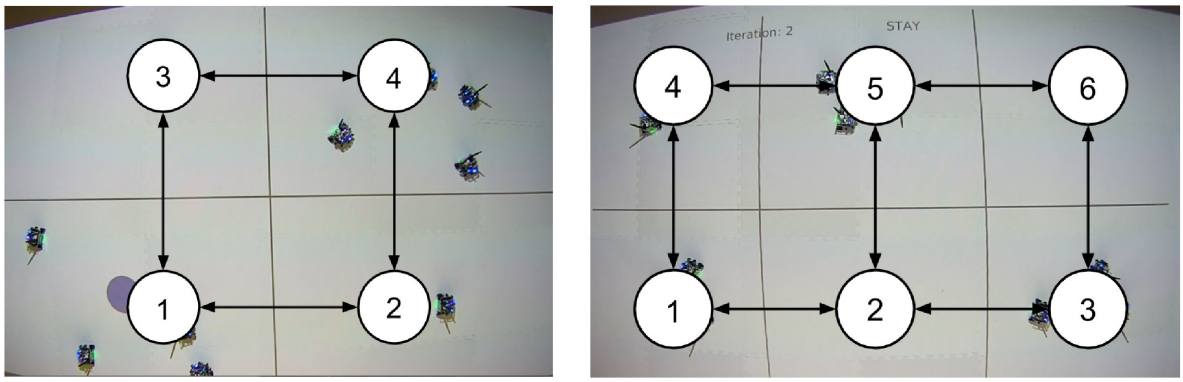

(a) (b)

Fig. 6. Initial setup of (a) Experiments 1 and 2, and (b) Experiment 3 on the Robotarium swarm robotics testbed, with the corresponding graph $\mathcal{G}$ superimposed.

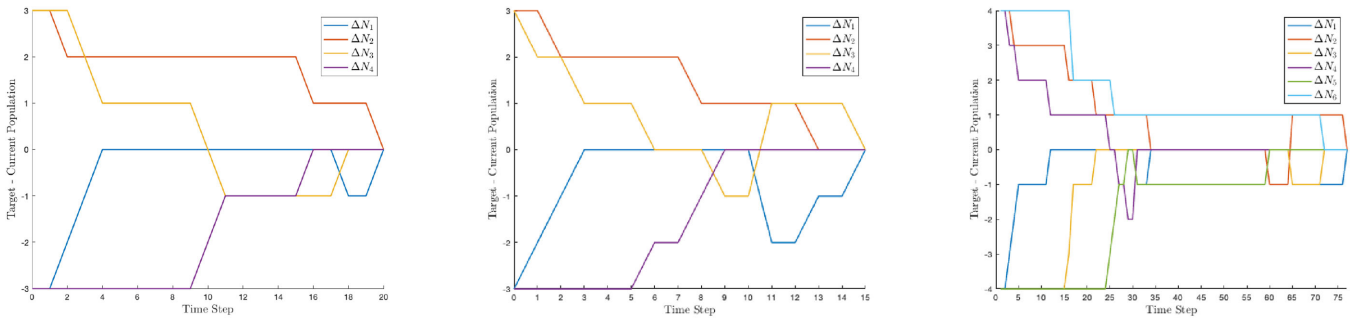

(a) (b) (c)

Fig. 7. Follower distribution over time in the Robotarium experiments with the closed-loop controller. (a) Experiment 1. (b) Experiment 2. (b) Experiment 3.

equal size, each of which corresponds to a vertex of the graph $\mathcal{G}$ (superimposed on the testbed). The initial and target follower agent distributions were defined as $N\mathbf{x}^0 = [4\,0\,4\,0\,4\,0]^T$ and $N\mathbf{x}^{\text{eq}} = [0\,4\,0\,4\,0\,4]^T$, respectively. The leader was able to herd the robots into the target distribution in 75 iterations, as shown in Fig. 7(a).

A movie of all three experiments is shown in the video attachment. In the video, the leader is red if it is stationary at its current state, and blue if it is moving to the next state in its path. The current time step k and leader action (either *Stay* if it is stationary, or the direction of its motion) are displayed at the top of the video frames.

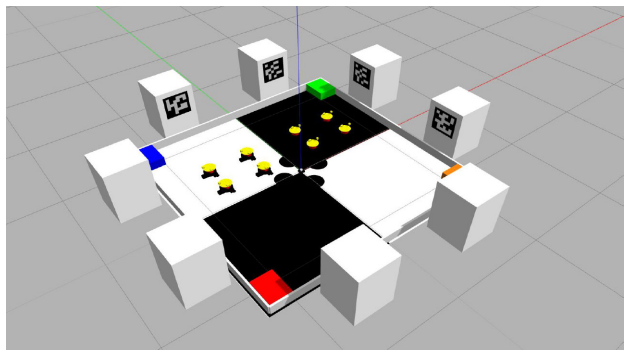

Fig. 8. Rendering of the 3-D simulation with a quadrotor (the leader) and eight Pheeno robots (the followers).

VIII. 3D MULTIROBOT SIMULATION RESULTS

We also validated the closed-loop controller (22) in a 3-D physics simulation with realistic leader and follower robot dynamics. We used the robot operating system to program the low-level and high-level control of the simulated robots in a completely decentralized manner, meaning that all robots take sensor measurements and decide on their next action autonomously, without the input of a supervisory agent or global observer. Additionally, each robot performs its computation and control independently of one another, with no interrobot communication. We used Gazebo [22] for 3-D simulation and rendering. The graph $\mathcal{G}$ and leader path $\mathcal{W}^\infty$ were the same as in the numerical simulations.

In the simulation, a quadrotor acts as the leader, and $N = 8$ *Pheeno* robots [39] act as the followers. Pheeno is a customizable, low-cost mobile robot developed by our laboratory. Each simulated Pheeno is equipped with an upward-facing sonar sensor and a ground-facing IR sensor. These sensors model the functionality of the HC-SR04 Ultrasonic Sensor and the QRE1113 Digital IR Sensor, respectively.

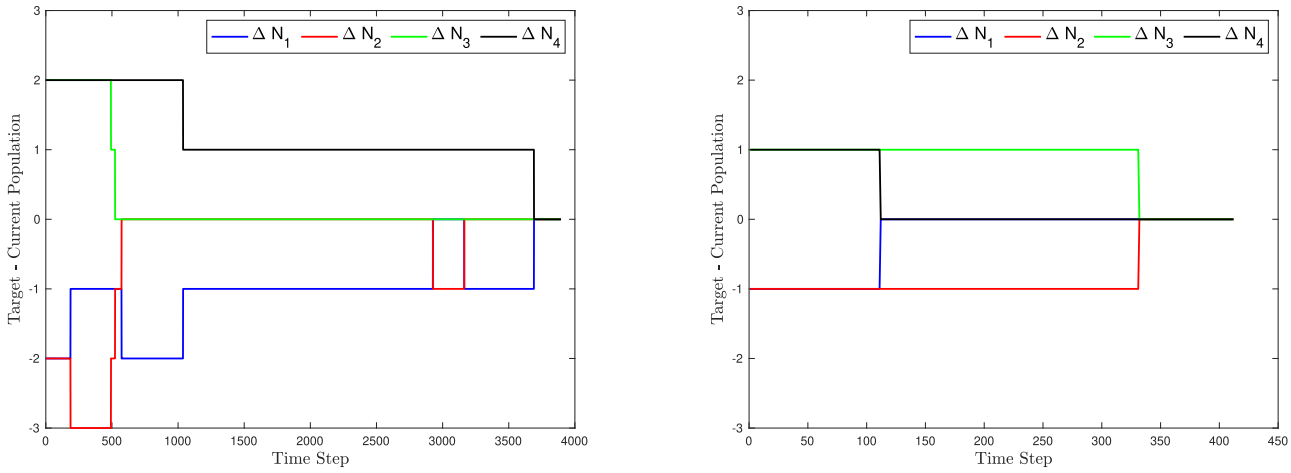

Fig. 9. Follower distribution over time in the 3-D simulation with the closed-loop controller. (a) Scenario 1. (b) Scenario 2.

The robots move within a 2.4 × 2.4 m bounded arena, shown in Fig. 8, that is divided into four black or white regions of equal size. Each region corresponds to a vertex of the graph $\mathcal{G}$. The regions contain different colored blocks that are used by the quadrotor to assist with its localization and to identify the region (state) over which it is flying: state 1 is green, state 2 is blue, state 3 is red, and state 4 is orange. The visual servo approach in [9] is used to localize the quadrotor with respect to the colored blocks in this way. The quadrotor determines the number of followers in its current state by counting the yellow circles on top of the Pheenos below. The eight pillars surrounding the arena are labeled with *ArUco* fiducial markers [35], which the Pheenos use to determine the heading to the next state in their transition. The two pillars that are adjacent to each region (state) have the same marker. Each Pheeno uses its ground-facing IR sensor to recognize when it has crossed into a new region by sensing the change in reflection that occurs when it travels from a white surface to a black surface, or vice versa. Each Pheeno also uses its upward-facing sonar sensor to detect the quadrotor when it is hovering at a low altitude above the Pheeno.

The closed-loop controller is implemented in the simulation as follows. The quadrotor moves according to (22) to enter the next state in the leader path, and it counts the number of Pheenos in that state. If this number is less than or equal to the target number, then the quadrotor moves to the next state in the path. If the number exceeds the target number, then the quadrotor descends, which triggers the sonar sensors on the Pheenos in that state. These Pheenos then transition to adjacent states, following (1). The quadrotor repeats these actions until the number of agents in each state equals the target number.

We performed two simulations of the closed-loop controller, each with different initial and target distributions. In *Scenario 1*, $N\mathbf{x}^0 = [4\,4\,0\,0]^T$ and $N\mathbf{x}^{\text{eq}} = [2\,2\,2\,2]^T$. In *Scenario 2*, $N\mathbf{x}^0 = [2\,2\,2\,2]^T$ and $N\mathbf{x}^{\text{eq}} = [1\,1\,3\,3]^T$. Fig. 9(a) and (b) plots the distribution of followers over time for both scenarios. The figures show that the closed-loop controller successfully drove the followers to the target distribution in each scenario.

IX. Conclusion

In this article, we addressed the problem of herding a robotic swarm to a desired distribution among a set of states using a leader agent that produces a repulsive effect on swarm members in its current state. We utilized a mean-field model of the swarm in our approach and establish approximate controllability of the model. Additionally, we constructed two switching feedback controllers for the leader agent. We proved that these controllers can stabilize the swarm to target probability distributions that are positive everywhere. Future work will focus on designing feedback laws and optimal control strategies for the leader agent that improve system performance criteria such as the rate of the follower agents' convergence to the target distribution and the robustness of this convergence to disturbances, such as environmental factors (e.g., wind) and interagent collisions. Another important problem to investigate is whether the empirical distribution of the N-agent Markov chain converges to the solution of the mean-field model in the case where leader's trajectory is a function of the follower distribution.

Acknowledgment

The authors would like to thank Dr. Sean Wilson at the Georgia Institute of Technology for running the robot experiments on the Robotarium.

References

[1] B. Açıkmeşe and D. S Bayard, "Markov chain approach to probabilistic guidance for swarms of autonomous agents," *Asian J. Control*, vol. 17, no. 4, pp. 1105–1124, 2015.

[2] S. Bandyopadhyay, S.-J. Chung, and F. Y Hadaegh, "Probabilistic and distributed control of a large-scale swarm of autonomous agents," *IEEE Trans. Robot.*, vol. 33, no. 5, pp. 1103–1123, Oct. 2017.

[3] A. Berman and R. J Plemmons, *Nonnegative Matrices in the Mathematical Sciences*, vol. 9. Philadelphia, PA, USA: SIAM, 1994.

[4] S. Berman, Á. Halász, M Ani Hsieh, and V. Kumar, "Optimized stochastic policies for task allocation in swarms of robots," *IEEE Trans. Robot.*, vol. 25, no. 4, pp. 927–937, Aug. 2009.

[5] Sp. Berman, V. Kumar, and R. Nagpal, "Design of control policies for spatially inhomogeneous robot swarms with application to commercial pollination," in *Proc. IEEE Int. Conf. Robot. Automat.*, 2011, pp. 378–385.
[6] Vladimir I Bogachev, *Measure Theory*, vol. 1. Berlin, Germany: Springer, 2007.
[7] A. Bressan and D. Zhang, "Control problems for a class of set valued evolutions," *Set-Valued Variat. Anal.*, vol. 20, no. 4, pp. 581–601, 2012.
[8] I. Chattopadhyay and A. Ray, "Supervised self-organization of homogeneous swarms using ergodic projections of Markov chains," *IEEE Trans. Syst., Man, Cybern., Part B*, vol. 39, no. 6, pp. 1505–1515, Dec. 2009.
[9] F. Chaumette and S. Hutchinson, "Visual servo control, Part I: Basic approaches," *IEEE Robot. Automat. Mag.*, vol. 13, no. 4, pp. 82–90, Dec. 2006.
[10] D. Cheng, "Controllability of switched bilinear systems," *IEEE Trans. Automa. Control*, vol. 50, no. 4, pp. 511–515, Apr. 2005.
[11] V. S Chipade and D. Panagou, "Herding an adversarial attacker to a safe area for defending safety-critical infrastructure," in *Proc. IEEE Amer. Control Conf.*, 2019, pp. 1035–1041.
[12] S. Chowdhury, W. Jing, and D. J Cappelleri, "Controlling multiple microrobots: Recent progress and future challenges," *J. Micro-Bio Robot.*, vol. 10, no. 1–4, pp. 1–11, 2015.
[13] R. M Colombo and N. Pogodaev, "Confinement strategies in a model for the interaction between individuals and a continuum," *SIAM J. Appl. Dyn. Syst.*, vol. 11, no. 2, pp. 741–770, 2012.
[14] M. Dunbabin and L. Marques, "Robots for environmental monitoring: Significant advancements and applications," *IEEE Robot. Automat. Mag.*, vol. 19, no. 1, pp. 24–39, Mar. 2012.
[15] K. Elamvazhuthi and S. Berman, "Mean-field models in swarm robotics: A survey," *Bioinspiration Biomimetics*, vol. 15, no. 1, 2019, Art. no. 015001.
[16] K. Elamvazhuthi, S. Wilson, and S. Berman, "Confinement control of double integrators using partially periodic leader trajectories," in *Amer. Control Conf.*, 2016, pp. 5537–5544.
[17] H. O Fattorini, *Infinite Dimensional Optimization and Control Theory*, vol. 54 Cambridge, U.K.: Press, 1999.
[18] R. Goebel, R. G Sanfelice, and A. R Teel, *Hybrid Dynamical Systems: Modeling, Stability, and Robustness*, Princeton NJ, USA: Princeton Press, 2012.
[19] M. A. Haque, A. R. Rahmani, and M. Egerstedt, "Biologically inspired confinement of multi-robot systems," *Int. J. Bio-Inspired Comput.*, vol. 3, no. 4, pp. 213–224, 2011.
[20] M. Ji, G. Ferrari-Trecate, M. Egerstedt, and A. Buffa, "Containment control in mobile networks," *IEEE Trans. Automat. Control*, vol. 53, no. 8, pp. 1972–1975, Sep. 2008.
[21] J. A Kirkland and A. A Maciejewski, "A simulation of attempts to influence crowd dynamics," in *Proc. IEEE Conf. Proc. Int. Conf. Syst., Man Cybern. Conf. Theme-Syst. Secur. Assurance*, vol. 5, 2003, pp. 4328–4333.
[22] N. P Koenig and A. Howard, "Design and use paradigms for Gazebo, an open-source multi-robot simulator," in *Proc. IEEE/RSJ Int. Conf. Intell. Robot. Syst.*, 2004, pp. 2149–2154.
[23] J. Li, B Esteban-Fernández de Ávila, W. Gao, L. Zhang, and J. Wang, "Micro/nanorobots for biomedicine: Delivery, surgery, sensing, and detoxification," *Sci. Robot*, vol. 2, no. 4, pp. 1–9, 2017.
[24] R. A Licitra, Z. I Bell, and W. E Dixon, "Single-agent indirect herding of multiple targets with uncertain dynamics," *IEEE Trans. Robot.*, vol. 35, no. 4, pp. 847–860, Aug. 2019.
[25] R. A Licitra, Z. I Bell, E. A Doucette, and W. E Dixon, "Single agent indirect herding of multiple targets: A switched adaptive control approach," *IEEE Control Syst. Lett.*, vol. 2, no. 1, pp. 127–132, Jan. 2018.
[26] A. Martinoli, K. Easton, and W. Agassounon, "Modeling swarm robotic systems: A case study in collaborative distributed manipulation," *Int. J. Robot. Res.*, vol. 23, no. 4–5, pp. 415–436, 2004.
[27] T William Mather and M Ani Hsieh, "Synthesis and analysis of distributed ensemble control strategies for allocation to multiple tasks," *Robotica*, vol. 32, no. 02, pp. 177–192, 2014.
[28] M. Mesbahi and M. Egerstedt, *Graph Theoretic Methods in Multiagent Networks*, vol. 33 Princeton NJ, USA: Princeton Press, 2010.
[29] A. A Paranjape, S.-J. Chung, K. Kim, and D. Hyunchul Shim, "Robotic herding of a flock of birds using an unmanned aerial vehicle," *IEEE Trans. Robot.*, vol. 34, no. 4, pp. 901–915, Aug. 2018.
[30] S. Park, Y. Oh, and D. Hong, "Disaster response and recovery from the perspective of robotics," *Int. J. Precis. Eng. Manuf.*, vol. 18, no. 10, pp. 1475–1482, 2017.
[31] D. Pickem *et al.*, "The Robotarium: A remotely accessible swarm robotics research testbed," in *Proc. Int. Conf. Robot. Automat.*, 2017, pp. 1699–1706.
[32] A. Pierson and M. Schwager, "Controlling noncooperative herds with robotic herders," *IEEE Trans. Robot.*, vol. 34, no. 2, pp. 517–525, Apr. 2018.
[33] A. Pierson and M. Schwager, "Bio-inspired non-cooperative multi-robot herding," in *Proc. Int. Conf. Robot. Automat.*, 2015, pp. 1843–1849.
[34] A. Renzaglia and A. Martinelli, "Potential field based approach for coordinate exploration with a multi-robot team," in *Proc. IEEE Saf. Secur. Rescue Robot.*, 2010, pp. 1–6.
[35] F. J. Romero-Ramirez, R. Muoz-Salinas, and R. Medina-Carnicer, "Speeded up detection of squared fiducial markers," *Image Vis. Comput.*, vol. 76, pp. 38–47, 2018.
[36] J. A Sanders, F. Verhulst, and J. Murdock, *Averaging Methods in Nonlinear Dynamical Systems*, vol. 59. Berlin, Germany: Springer, 2007.
[37] Z. Sun, S. Sam Ge, and T. Heng Lee, "Controllability and reachability criteria for switched linear systems," *Automatica*, vol. 38, no. 5, pp. 775–786, 2002.
[38] T. Rex Trumbull and S. Rene Myrtle, "Unmanned livestock monitoring system and methods of use," U.S. Patent App. 15/000,018 Jul. 20 2017.
[39] S. Wilson *et al.*, "Pheeno, a versatile swarm robotic research and education platform," *IEEE Robot. Automat. Lett.*, vol. 1, no. 2, pp. 884–891, Jul. 2016.
[40] L. Chisholm Young, *Lecture on the Calculus of Variations and Optimal Control Theory*, vol. 304. Providence, RI, United States: American Mathematical Soc., 2000.

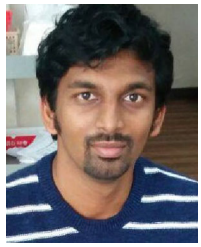

Karthik Elamvazhuthi received the B.Tech. degree in mechatronics engineering from the Manipal Institute of Technology, Manipal, India, in 2011 and the M.S. and Ph.D. degrees in mechanical engineering from Arizona State University, Tempe, AZ, USA, in 2014 and 2019, respectively.

He is currently a CAM Assistant Adjunct Professor with the Department of Mathematics, University of California, Los Angeles, CA, USA. His research interests include modeling and control of robotic swarms using methods from partial differential equations and stochastic processes.

Zahi Kakish received the B.S. degree in mechanical polymer engineering from the University of Akron, Akron, OH, USA, in 2013 and the M.S. degree in mechanical engineering from the University of Akron, in 2015. He is currently working toward the Ph.D. degree in mechanical engineering with Arizona State University, Tempe, AZ, USA.

His research interests include swarm intelligence, human–swarm interaction, and multiagent reinforcement learning.

Aniket Shirsat received the B.E. degree in mechanical engineering from the University of Mumbai, Mumbai, India, in 2010 and the M.S. degree in mechanical engineering in 2015 from Arizona State University, Tempe, AZ, USA, where he is currently working toward the Ph.D. degree in mechanical engineering.

His research focuses on distributed perception and exploration in robotic swarms.

Spring Berman (Member, IEEE) received the M.S.E. and Ph.D. degrees in mechanical engineering and applied mechanics from the University of Pennsylvania, Philadelphia, PA, USA, in 2008 and 2010, respectively.

From 2010 to 2012, she was a Postdoctoral Researcher in Computer Science with Harvard University, Cambridge, MA, USA. Since 2012, she has been a Professor of Mechanical and Aerospace Engineering with Arizona State University, Tempe, AZ, USA. Her research focuses on the analysis of behaviors in biological and engineered collectives and the synthesis of control strategies for robotic swarms.

Prof. Berman was a recipient of the 2014 DARPA Young Faculty Award and the 2016 ONR Young Investigator Award.